Numerical analysis of compressed components of beam-to-rectangular hollow section column moment resistant steel joints

Author: Margarita Mikheeva

Supervisor: Prof. Dr. Rui António Duarte Simões

University: University of Coimbra

University: University of Coimbra
Date: 31.01.2017

ABSTRACT

Hollow sections appear to be very attractive from the architectural and structural point of view. They exhibit high aesthetic performance along with significant resistance to compression, bending and torsion. Additionally, hollow sections show higher durability and corrosion resistance comparing to opened sections.

However, connecting to hollow sections is a demanding procedure. The absence of the access to the interior void of hollow sections leads to the necessity of developing appropriate types of joints which would allow to balance design, fabrication, erection and operation stages with the overall project cost.

The range of possible connections of beams to hollow sections is already invented. Nevertheless, there is always a challenge to develop connection types with improved characteristics.

The present thesis is a part of the wider research of beam-to-rectangular hollow section column moment resistant joint subjected mainly to the action of the bending moment. The main research project is divided into three parts, investigation of compressed components of the joint, tension components of the joint and the entire joint behaviour. Each part contains experimental tests, numerical modeling and analytical characterization of the joint behaviour.

The goal of the thesis is to investigate the behaviour of compressed components of the joint by numerical modeling. Numerical results are further validated by comparison to experimental data.

Numerical simulations are carried out by *DS Simulia Abaqus* software. The thesis includes numerical analysis of four models corresponding to experimental specimens which represent compressed components of the joint. After the calibration of obtained results the parametric study is implemented for 104 numerical models more. The parametric study aims to investigate the behaviour of the components for the extended range of geometrical variation.

The result of the present thesis is the information about resistance and stiffness of the compressed components of the joint based on the force - displacement response which is obtained for the total number of 108 numerical models.

Keywords: hollow sections, moment resistant joints, channel joints, compressed component, numerical analysis.

TABLE OF CONTENTS

LIST OF TABLES

LIST OF FIGURES

NOTATION

B	The U-section flange width
E	The elastic modulus
F_{Rd}	The design resistance
I_b	The second moment of area of a beam cross-section
I_c	The second moment of area of a column cross-section
K_b	The mean value I_b/L_b for all the beams at the top of the storey
K_c	The mean value I_c/L_c for all the columns in the storey
K_e	The elastic stiffness
L_b	The span of a beam (centre-to-centre of columns)
L_c	The storey height of a column
L_{load}	The loading plate length
$M_{b,pl,Rd}$	The design plastic moment resistance of a beam cross-section
$M_{c,pl,Rd}$	The design plastic moment resistance of a column cross-section
$M_{j,Rd}$	The design moment resistance of a joint
S_j	The rotational stiffness of a joint
$S_{j,ini}$	The initial rotational stiffness of a joint
h	The U-section height
h_r	The distance from bolt row in tension to the centre line of compressed zone
k	The stiffness coefficient
k_{eff}	The effective stiffness coefficient
k_{eq}	The equivalent stiffness coefficient
t	The U-section thickness
z_{eq}	The equivalent lever arm
Δ	The displacement
β_1	The value of the transformation parameter β for the right side joint
β_2	The value of the transformation parameter β for the left side joint
ε	The strain
ε_{nom}	The nominal strain
ε_{pl}	The plastic strain
ε_{true}	The true strain
η	The stiffness modification coefficient
σ_{nom}	The nominal stress
σ_{true}	The true stress
ϕ	The rotation of the joint

ABBREVIATION

CHS	Circular Hollow Section
CIDECT	Comité International pour le Développment et l'Etude de la Construction Tubulaire
FE	Finite Element
FEA	Finite Element Analysis
FEM	Finite Element Model
RFCS	Research Fund for Coal and Steel
RHS	Rectangular Hollow Section
SHS	Square Hollow Section

1.INTRODUCTION

1.1. Overview behaviour

The present thesis is a part of a wider research project of the beam-to-rectangular hollow section column moment resistant joint.

The research program aims to investigate the behaviour of beam-to-column joint subjected mainly to the action of the bending moment. The column is represented by a rectangular hollow section and a beam is represented by an I-section profile. Connection is implemented with a usage of two U-sections, welded end plates and bolts.

The main research project is divided into three global parts, investigation of compressed components of the joint, tension components of the joint and the behaviour of the whole joint. Each part contains experimental tests, numerical modeling and analytical characterization of the joint behaviour.

The present thesis has a goal to investigate the behaviour of the joint compressed components by numerical modeling and compare results to experimental data.

Numerical simulations are carried out by *DS Simulia Abaqus* software. The thesis includes modeling of four test specimens which represent the compressed components of the joint. After the validation of obtained results, the numerical simulation of 104 numerical models more is implemented in order to investigate the behaviour for the extended range of the geometrical variety of the beam-to-RHS column joint.

Design of connections plays a significant role in a structural behaviour design. Moreover, well-designed connections allow to decrease time of erection process and reduce total price of a project.

High interest to this type of connection is a consequence of hollow section advantages. In the recent history of engineering hollow sections are widely used due to their architectural performance. In addition, structural behaviour of closed sections surpasses behaviour of opened sections by virtue of higher resistance to bending and torsion. Furthermore, hollow sections show higher durability and corrosion resistance due to reduced area of protection and absence of sharp corners.

To sum up all the advantages, they are listed below.

Advantages of hollow sections:

- High performance of resistance to compression, torsion and bending in all direction,
- Architectural attractiveness,
- Closed shape leading to decrease of corrosion protected area,
- Absence of sharp corners as a positive factor in terms of fatigue and corrosion,

- Lower drag coefficients if exposed to wind and water forces,
- Possibility of internal cavity usage for different applications, such as fire protection or increase of resistance capacity by concrete filling.

Considering the increasing popularity of hollow sections and their further perspectives it is important to notice that over recent time the vast amount of researches was performed. As a result, design codes and recommendations were significantly improved [Puthli, 2001]. Nevertheless, yet there is a lack of clearly stated procedure of the present joint type design. The deficiency of information should be filled with precise guidelines in order to facilitate design process for application amongst structural engineers.

The principal idea of the global research is to provide a procedure to analyse and design this type of joints based on the component method as well as to invent simple expressions for characterization of the joint basic components behaviour. Thus, the main goal of the global research is to develop a reliable design procedure.

1.2. Brief contents

The present thesis consists of 5 chapters. Brief contents of each chapter are listed as follows.

Chapter 1. Introduction

In Chapter 1, the overall introduction to the subject of the thesis is described along with the brief overview of the main goal and the main concept of the present work.

Chapter 2. State of the art

In Chapter 2, the development and the use of structures with hollow sections are described. It comprises a historical overview along with pointing out to main advantages of hollow sections. It follows by the description of the most recent researches which are dedicated to the study of the behaviour of connections to hollow sections.

Additionally, Chapter 2 covers the concept of the joint design. The key point of the joint design, so-called component method is also highlighted along with its trustworthiness and simplicity of application in designing process.

Chapter 3. Experimental work

In Chapter 3, the beam-to-RHS column joint is described, i.e. the joint behavior and joint basic components based on the concept of the component method. In this Chapter, experimental results of compression tests are provided.

Chapter 4. Numerical simulations

In Chapter 4, the description of numerical simulations of the joint compressed components is provided. Finite element analysis is carried out using *DS Simulia Abaqus* software. All main

parts of finite element modeling are specified, such as mesh study, validation of the numerical model etc. Results of FEA and comparison to the experimental data are presented.

Furthermore, results obtained by the parametric study are provided in this Chapter.

Chapter 5. Conclusion

In Chapter 5, the main conclusions of the present thesis are listed along with the overview of the future work and further perspective from the point of view of the contribution of the present thesis to the research project.

2.STATE OF THE ART

2.1. History of development of hollow sections

Preeminent properties of closed shaped sections are known since ancient time. Our ancestry discovered them by watching natural examples, such as bamboo or reed. These plants performed a good behaviour in terms of compression, torsion and bending resistance.

Human-built examples of hollow section structures application are known for a very long time, e.g. the Firth of Forth Bridge in Scotland with a free span of 521 metres dated by 1890 (Figure 2.1). The bridge was constructed using tubular hollow sections made of rolled plates made up together by rivets according to possible fabrication process known at that time.

Figure 2.1 Firth of Forth Bridge in Scotland.

Manufacturing process of seamless and welded circular hollow sections got a significant motion in late XIX century by developing the skew roll piercing process by Mannesmann brothers (Figure 2.2). The process allowed to roll short thick walled tubular sections. Few years later the pilger process (Figure 2.3) was developed which in a combination with skew roll piercing process made it possible to produce longer thinner walled seamless hollow sections [Wardenier *et al.*, 2010].

Later on, in the beginning of XX century Whitehouse invented the fire welding of circular hollow sections. Then, in 1930 Fretz Moon developed the continuous welding process which allowed to easily weld hollow sections together [Wardenier *et al.*, 2010] (Figure 2.4).

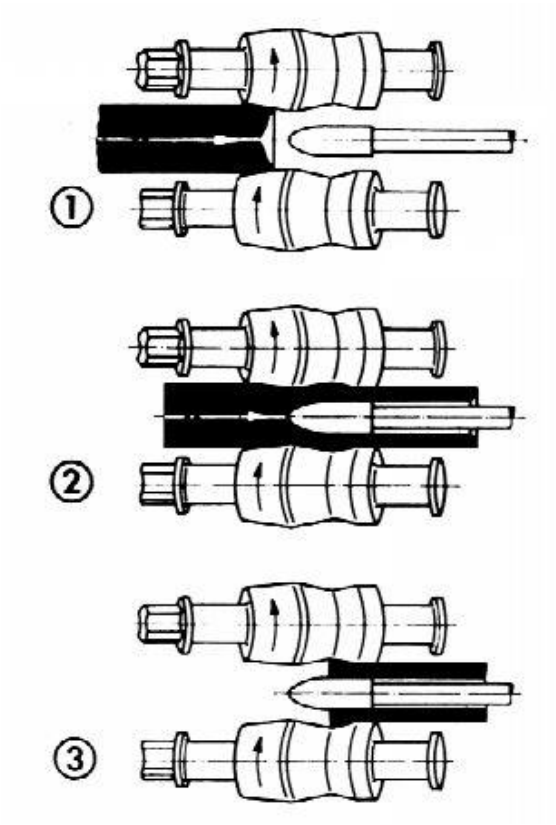

Figure 2.2 Skew roll piercing process [Wardenier *et al*., 2010].

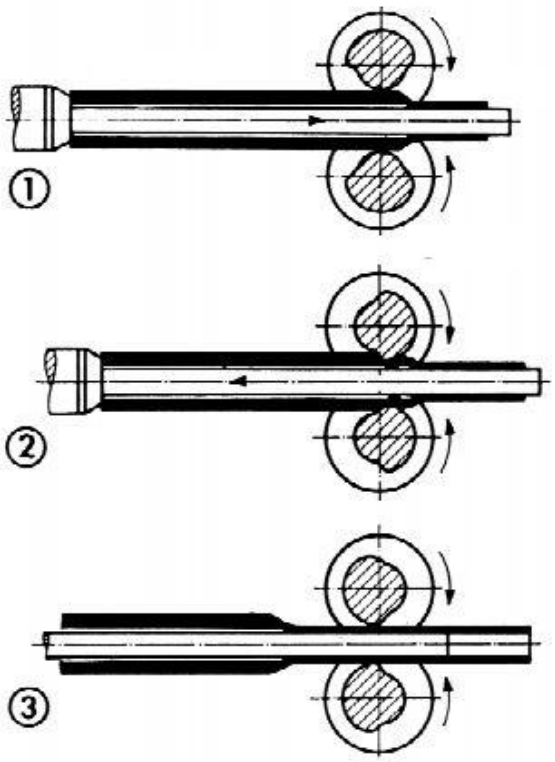

Figure 2.3 Pilger process [Wardenier *et al*., 2010].

The next development of the hollow sections fabrication was done by Muller who evolved the end cutting process required for fitting two circular hollow sections. The main idea was in the special end treatment made by the end preparation machine [Wardenier *et al*., 2010] (Figure 2.5).

Then, in 1937 Mengeringhausen developed the Mero system. Elaboration of this prefabricated connector resolved production of space structures in an industrialized way (Figure 2.6).

In 1952, the rectangular hollow section was developed by Stewarts and Lloyds, nowadays Corus Tubes. The possibility of making connections of rectangular hollow sections by straight end cuttings made an advantage comparing to the circular hollow section [Wardenier *et al*., 2010].

By this time, manufacturing, end preparation and welding processes were significantly developed. The remaining issue was the definition of the strength of unstiffened joints.

The lack of design recommendations inspired researches to study truss connections between circular hollow sections. The first research was done by Jamm in 1951 [Wardenier *et al*., 2010]. His interest to hollow sections was followed by researches from all over the world, such as Europe, USA, Japan.

Investigation of joints between rectangular hollow sections started in Europe ten years later, in the sixties.

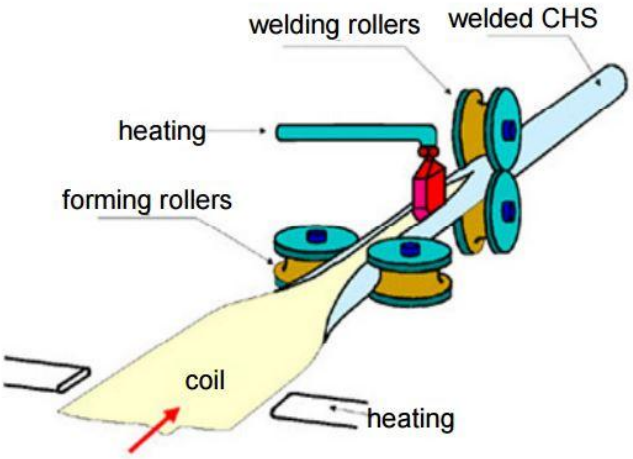

Figure 2.4 Fretz Moon continuous welding process [Wardenier *et al*., 2010].

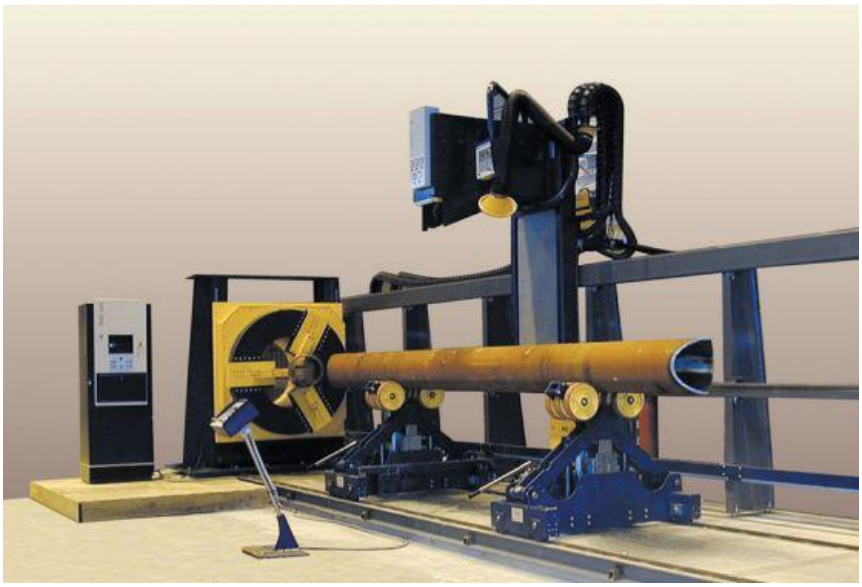

Figure 2.5 End cutting machine [Wardenier *et al*., 2010].

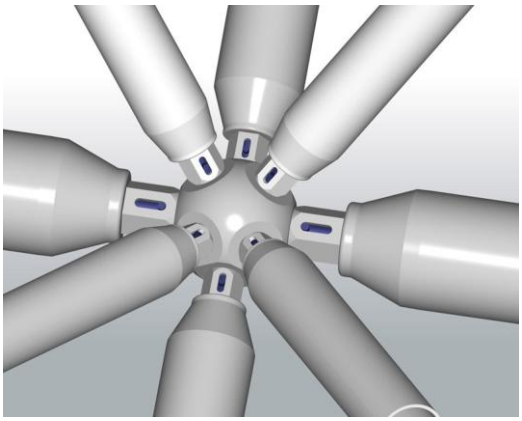

Figure 2.6 Mero connector.

Later on, the manufacturers and researches society founded an international association of leading manufacturers of hollow sections and pipes, CIDECT. It significantly impacted the development of this area by expanding knowledge, financing of researches and experiments and promotion of innovative achievements to fabrication and construction.

CIDECT association published a number of design guides for structural engineers in order to facilitate design of the most common hollow sections applications. However, engineering is a constantly developing area what leads to appearance of new challenges in the field of hollow sections application and sequential necessity of new researches.

2.2. Recent researches of hollow section joints

2.2.1. Overview

Considering the attractiveness of beam-to-hollow section columns, this type of connection has been studied already by many research teams. Summarising their contribution, two types of connection are mostly adopted to practice, namely connection with special bolts, e.g. blind bolts directly connected to a column wall, and connection with reversed channel (Figure 2.7). Both of them have the advantage in terms of erection process due to avoiding direct access to the internal void of hollow section.

In the present clause, several recent researches are highlighted. All of them aim to investigate a behaviour of beam-to-column connections where columns are represented by hollow sections and beams are either RHS or I-beams.

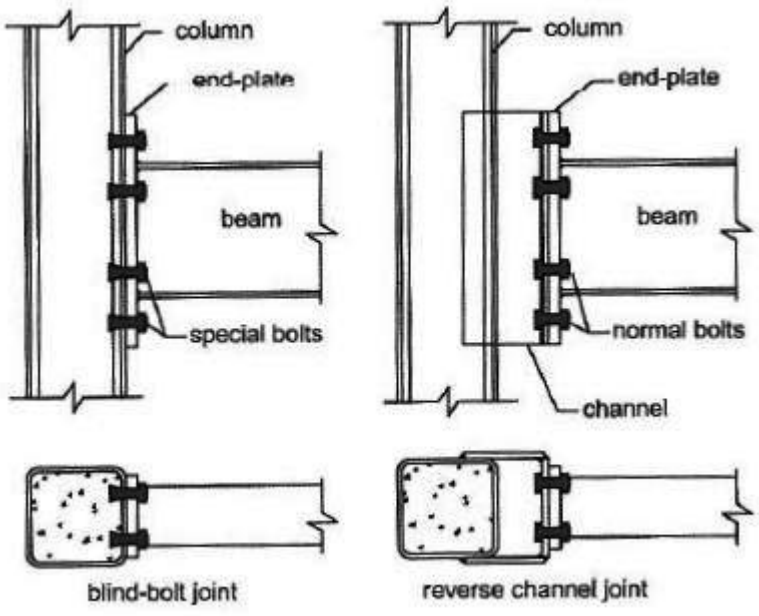

Figure 2.7 Most common solutions for beam-to-hollow section column joints.

2.2.2. Behaviour of RHS beam-to-column bolted steel connections

The research of Barros dos Santos, Miranda Batista and Mascarenhas de Araujo is dedicated to behaviour of RHS beam-to-column bolted steel connections [Barros dos Santos *et al*., 2016] (Figure 2.8).

The purpose of the research is to describe a new typology of beam-to-column connections which integrates simple fabrication and erection with structural effectiveness. In order to improve aesthetic aspect of the joint internal cleat plates were introduced.

Four cruciform prototypes were tested under a static non-reversible bending moment using different types of bolted connections, such as non-friction and friction connections.

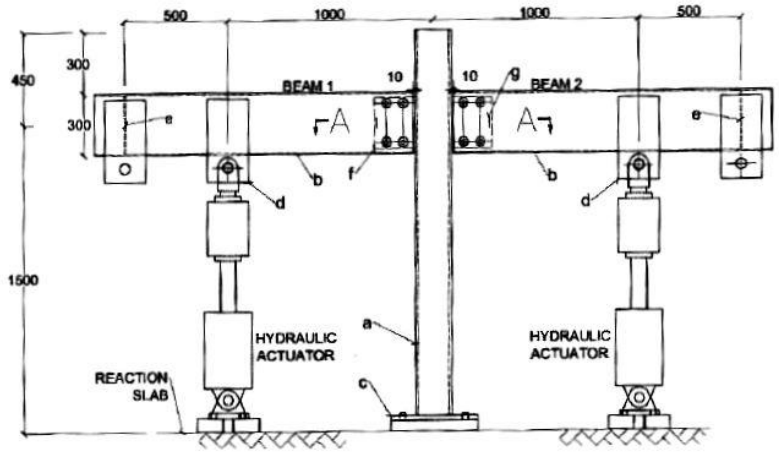

Figure 2.8 Test setup [Barros dos Santos *et al*., 2016].

The moment-rotation response is obtained by the relative rotation between the beam and the column.

The measurements show that beams confirmed linear-elastic behaviour during all the tests and columns had elastic deformations with a small non-linear contribution, apparently due to local plate bending. Cleat plates performed large deformations. Non-friction type prototypes presented a rigid behaviour for bending moment up to 13 kNm while friction type connections performed a rigid behaviour up to 40 kNm (Figure 2.9).

Experimental results demonstrate that the friction connection is able to develop a rigid elastic moment-rotation response up to usual loading conditions. The following goal of the researchers is to investigate the friction-type connection behaviour under reversed bending moment.

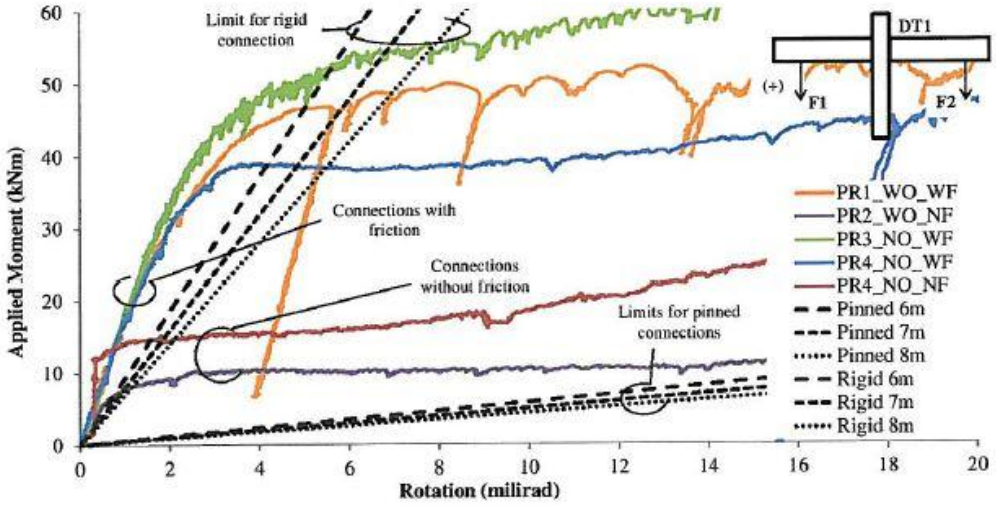

Figure 2.9 Bending moment-rotation response of all tests [Barros dos Santos *et al*., 2016].

2.2.3. Long bolts for beam to concrete filled RHS column joints in seismic-resistant frames

Another research was done by Hoang, Jaspart and Demonceau. It aimed to investigate the use of long bolts for beam to concrete filled RHS column joints in seismic-resistant frames [Hoang *et al*., 2016] (Figure 2.10).

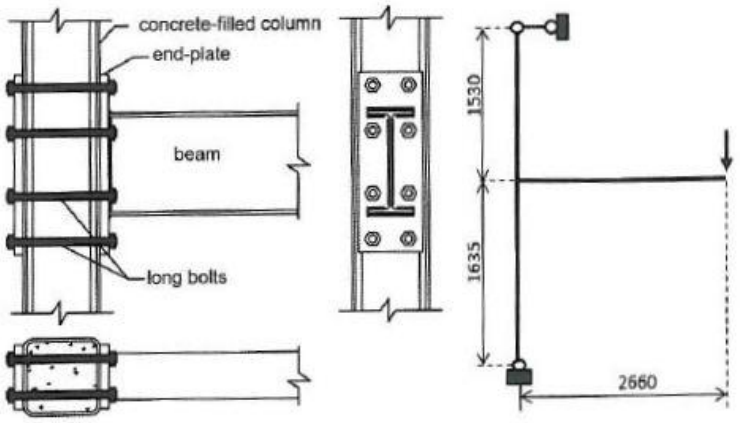

Figure 2.10 Joint configuration and test setup [Hoang *et al*., 2016].

The aim of the research is to investigate the behaviour of I-beam to RHS column joint made up with long bolts passing through the column. The purpose of long bolts is to avoid additional connecting elements and, in addition, to improve the resistance and stiffness of the joint under seismic load of medium to strong earthquake.

Bolts are preloaded according to recommendations of EN 1090-2 [CEN, 2008]. Tests show that preloading stays active until the end of the test. This fact is displayed by load-

displacement curves where it can be noticed that the joint stiffness remains until the plastic hinges develop in the beam (Figure 2.11).

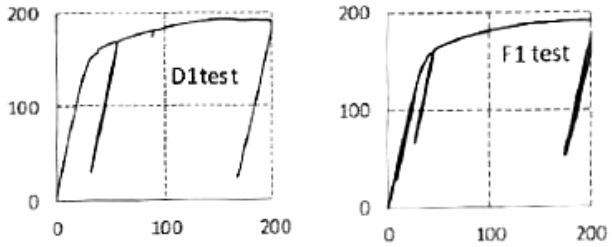

Figure 2.11 Load-displacement curves of joints under monotonic load [Hoang *et al*., 2016].

Note: D1 - Column SHS 300x300x12.5 grade S460, F1 - Column SHS 250x250x10 grade S700.

From the tests it was observed that joints perform reasonably high stiffness under bending and high shear resistance.

Experimental results were validated by comparison with analytical solution which combines component method stated in EN 1993-1-8 [CEN, 2005] with the proposal for unmentioned components of the joint, e.g. shear resistance of long bolts, bearing resistance of concrete core. Although there are unmentioned components of the joint, using few additional rules all components can be determined by application of component method stated in EN 1993-1-8 [CEN, 2005].

Thus, the proposed configuration of the joint represents a good solution for high-resistance beam-to-column joint which allows to avoid additional connecting elements. Nevertheless, there is complexity related to the erection process on construction site using long bolts connections and also related to the implementation of the connection in two horizontal directions.

2.2.4. Cyclic behaviour of external diaphragm joint to CHS column with built-in replaceable links

Another research was done in 2016 by Khador and Chan. It aims to investigate cyclic behaviour of external diaphragm joint to CHS column with built-in replaceable links [Khador and Chan, 2016].

The experimental work is based on the numerical investigation made by Sabbagh [Sabbagh *et al*., 2013]. Previously, several researches were done by different authors but joint stiffness was rather low due to geometry. The research of Sabbagh determined structural weakness of the joint and proposed a solution which allows to develop a plastic hinge in a dog-bone cover plates while column wall and beam show elastic behaviour. The advantage of the joint is a possible replacement of components suffered seismic actions.

Khador and Chan made an experimental work to identify if the joint performes a higher stiffness. The joint contains of CHS column with two welded diaphragm plates. Plates are bolted to I-beam flanges using cover plates and to the beam web using web stub plate (Figure 2.12).

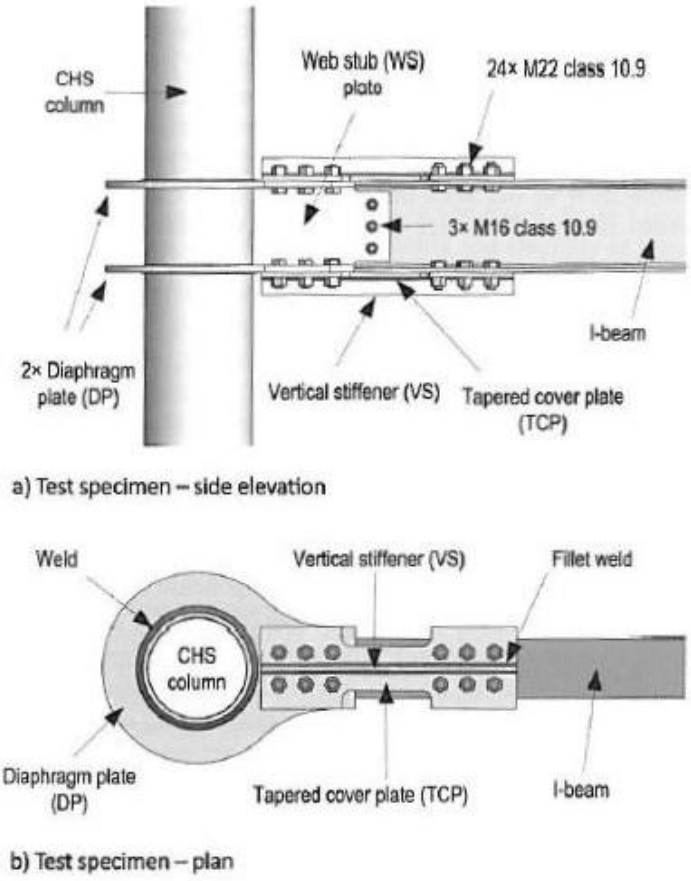

Figure 2.12 Test specimen [Khador and Chan, 2016].

Experimental results show that yielding occurred in the reduced section of tapered cover plates which caused a development of a plastic hinge whilst other components of the joint performed elastic behaviour.

By the initial rotational stiffness the joint was classified as a semi-rigid joint for all three tests.

Maximum plastic hinge rotation was 21.1 mrad for the specimen with full preloaded bolts and 25.8 mrad for the specimen with half preloaded bolts. It shows that the slip activation increase the energy dissipation which increases rotation capacity of the joint. Thus, considering slip activation the joint can be applicable for medium ductility class structures (DCM) as the rotational capacity of the plastic hinge is more than 25 mrad.

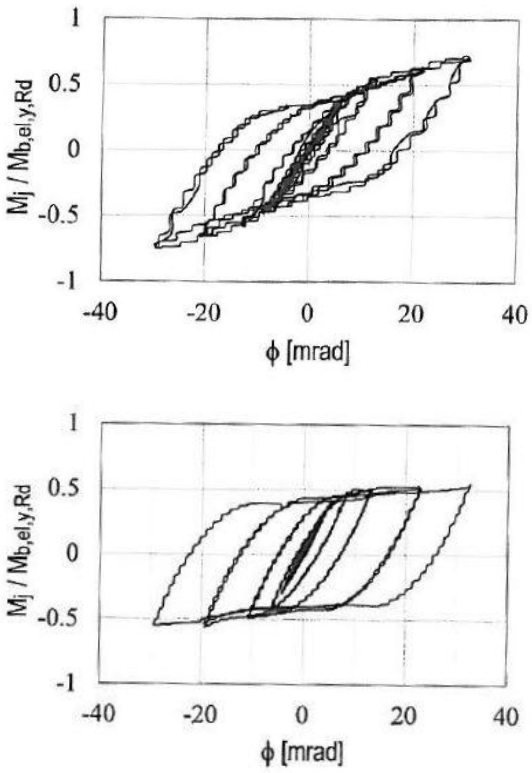

a) Test of specimen applying full preloading of bolts for slip-resistant connections according to EN 1993-1-8 [CEN, 2005]. Bolt holes are oversized.

Number of cycles: 30.

b) Test of specimen applying half preloading of bolts. Bolt holes are oversized.

Number of cycles: 30.

Figure 2.13 Normalized moment-rotation curve of the joint [Khador and Chan, 2016].

As a conclusion, the joint develop a plastic hinge in the cover plate what allows to classify the joint as applicable for seismic areas with possibility of minimal post-seismic repair. Also due to adequate rotational capacity of the plastic hinge the joint can be used for DCM structures.

2.2.5. Experimental behaviour of the reverse channel joint component at elevated and ambient temperatures

The experimental investigation of the reverse channel component was carried out by Lopes, Santiago, Simoes da Silva, Heistermann, Veljkovic and da Silva as part of European RFCS COMPFIRE Project which aims to investigate the behaviour of steel joints that connect steel beams to concrete-filled tubular (CFT) columns under natural fire loading [Lopes *et al*., 2013].

A series of tensile and compressive tests at ambient and elevated temperatures was implemented in order to characterise the strength, stiffness and ductility of this joint component.

The geometry and also active basic components of the joint are shown in the Figure 2.14. Components 1 to 7 and 11 to 13 are defined in EN 1993-1-8 [CEN, 2005], component 10 (column wall in bending) is not included in the Eurocode yet although there are CIDECT guidelines and several works which cover stiffness of the component [Jaspart et al., 2005], [Simoes da Silva et al., 2011]. Components 8 (reverse channel in bending) and 9 (reverse

channel in compression) are not covered in the literature, thus the set of analytical and numerical analysis along with experimental work was carried out by the authors.

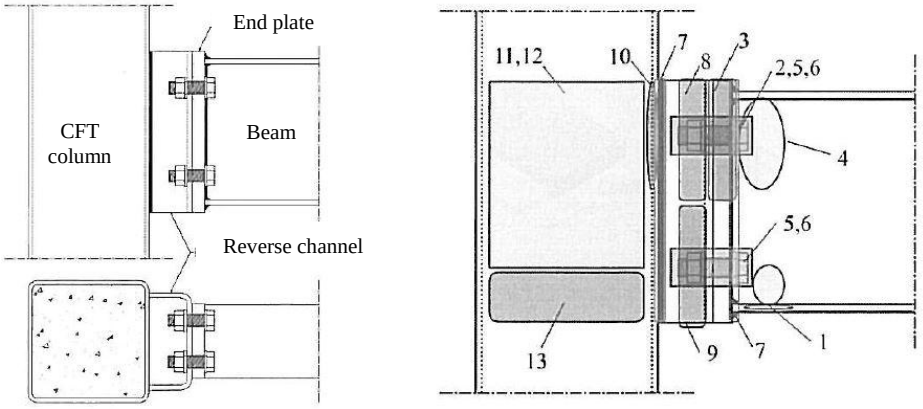

Figure 2.14 Reverse channel joint: geometry and basic joint components [Lopes *et al*, 2013].

The reverse channel as a basic component exhibits the following load transfer mechanism: a tensile zone is around top bolt row and a compression zone around the beam bottom flange. In general, it's behaviour is similar to the column web in transverse bending/compression in end-plate weak-axis joints. The difference is the influence of the reverse channel flanges to the bending behaviour of the column loaded wall and the limited length of the reverse channel. Thereby, the authors studied the behaviour of the reverse channel in order to establish if the existing approach is suitable for the reverse channel as a component.

The experimental program consisted of 13 tensile and 8 compressive tests under the monotonic load applied to U-sections transversally at the ambient temperature and also at 550°C and 750°C. Three types of U-section were tested under tension: built-up sections from welded plates, steel hollow sections cut lengthwise and hot-rolled UPN 200 profile. Compression tests were performed for welded sections.

Tensile tests showed that the strength of the U-section increased with increasing web thickness, however UPN section performed better results in terms of resistance. Initial stiffness increased with increasing web thickness as well. Ductility was similar for all tensile tests. The maximum vertical displacement reached 60 mm. Measured in the web strains indicate the beginning of the yielding around bolts' holes. The propagation of the yielding was observed then to the middle of the web and to free edges of specimens.

Specimens in compression present significantly higher strength and initial stiffness than ones in tension. Although, higher deformations are reached in tension (Figure 2.15). Under compression load the yielding initiated close to the flanges coinciding with the edges of the load device.

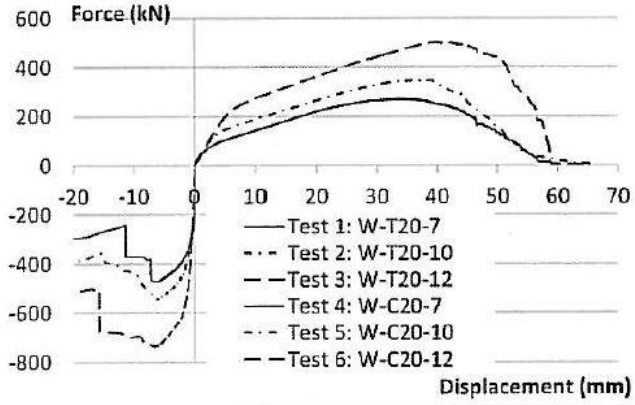

Figure 2.15 Tensile and compressive tests at ambient temperature of welded plate sections [Lopes *et al.*, 2013].

Observed failure modes in tension and compression tests were bolts punching through the holes without bolts failure and shear failure on the web next to flanges aligned with the edge of the compressive device, respectively. Deformed shapes are depicted in the Figure 2.16.

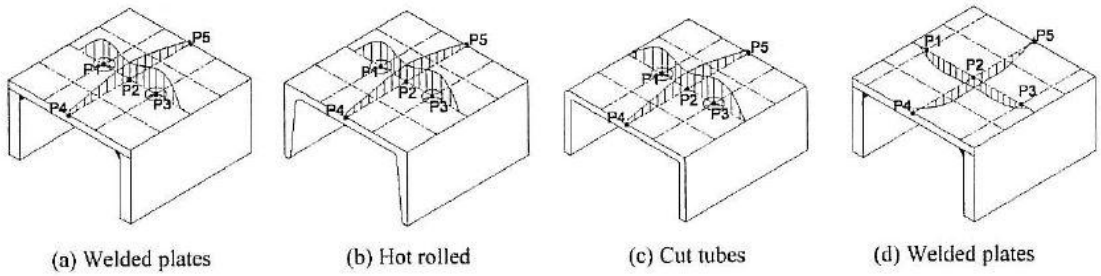

Figure 2.16 Deformed shapes of specimens after tensile tests (a to c) and compressive tests (d) [Lopes *et al.*, 2013].

Experiments at elevated temperatures show significant degradation of the material properties what strongly affects the resistance, e.g. for 750°C it was about 10% of the resistance at ambient temperature. Also the bad influence was observed in the reduction of the stiffness, both initial and post-limit. Failure modes at elevated temperature were similar to those observed at ambient temperature.

It may be concluded that the geometry of the reverse channel and the overall experimental output proof that analytical models available in the literature nowadays cannot be applied to the reverse channel as a basic joint component. Thus, a new analytical model should be evaluated.

2.2.6. Moment resisting bolted joints connecting steel tubular sections

The research of the reverse channel beam-to-RHS column connection under static, cyclic and fire load is carried out by Vicente, Simoes, Rebelo etc. in the frame of European RFCS FRAMEUP project [Vicente *et al*., 2014].

The main goal of the work is to investigate the behaviour of reverse channel component to be further included in the assembly of the joint by implementation of the component method. The paper is dedicated to the results obtained by numerical analysis and experimental tests.

Experimental part of the work consisted of testing 4 specimens representing joints submitted to a negative bending moment. Each prototype was composed by the column SHS 250x10 and the beam RHS 250x150x8 connected by the reverse channel made of longitudinally cut SHS 250x10 section. Bolts M27 (10.9) connected the beam to the channel through the end-plate (Figure 2.17). Corresponding numerical models were developed.

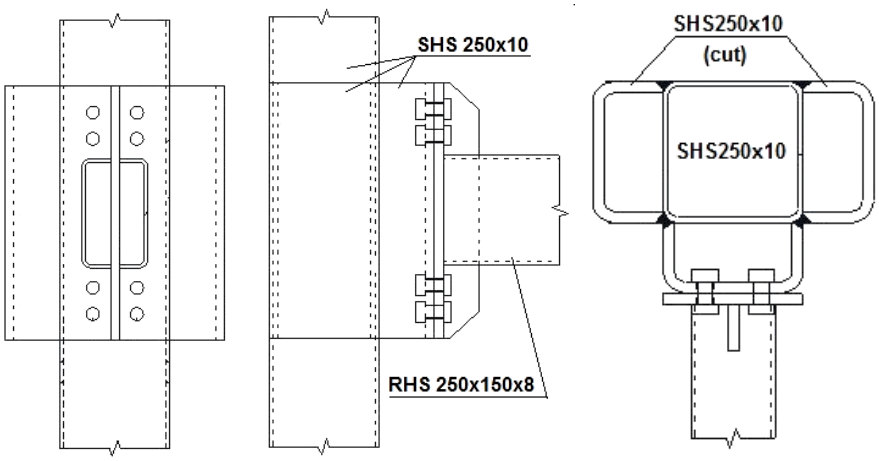

Figure 2.17 Geometry of the reverse channel joint [Vicente *et al*., 2014].

As the result of the work, the moment - rotation response of the joint was obtained both numerically and experimentally. Moment - rotation curves are presented in the Figure 2.18. Analysing the results the authors conclude that increase of the thickness of the reverse channel or the end-plate leads to increase of the rotational stiffness of the joint. The moment resistance of the joint is influenced by increase of the thickness as well. In addition, in all the tests the beam was indicated to remain the weakest component.

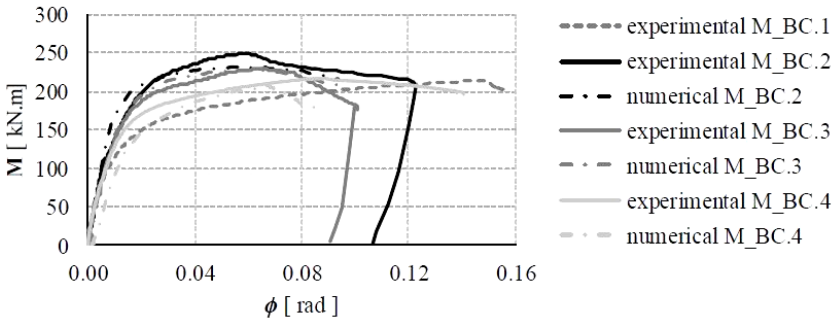

Figure 2.18 Moment - rotation curves [Vicente *et al*., 2014].

The further work includes the characterisation of all new basic joint components with the subsequent evaluation of the analytical approach in order to facilitate the design procedure and supplement Eurocode 3 with the recommendations for this type of the joint .

2.3. Design of joints

2.3.1. General

Nowadays, connections with hollow sections are mostly performed by bolted and welded solutions. The design should be balanced between safety and total cost. Total cost is affected by application of additional stiffeners, timing and erection processes, e.g. welding on construction site is more complicated and costly option comparing to usage of bolted connections.

Available design recommendations of hollow section joint are stated in Chapter 7 of EN 1993-1-8 [CEN, 2005]. The guidelines are referred to determination the static design resistances of uniplanar and multiplanar welded joints in lattice structures composed of circular, square or rectangular hollow sections and of uniplanar joints in lattice structures composed of combinations of hollow sections with open sections.

Another source of design recommendations are CIDECT design guides which in general deal with design of hollow sections. The hollow section joint design is accumulated in Design Guide 3 "Design guide for rectangular hollow section joints under predominantly static loading" [Packer *et al*., 2009], Design Guide 9 "Design guide for structural hollow section column connections" [Kurobane *et al*., 2004].

Regarding the design of connections, all joints should be designed following the procedure:

- Characterisation of the joint using component method,
- The joint modeling,
- The joint classification (by stiffness, strength and ductility),
- The joint idealisation.

2.3.2. Component method for joints

The component method allows to design joints of any configuration considering a joint as a set of basic components, i.e. each part of a joint is a joint basic component. Thus, the component method can be implemented for joints of any geometry and the connection type such as welded and bolted connections.

The component method is widely applicable to define stiffness and strength of connections which are predominantly moment-resisting connections. The mechanical behaviour of all the components is evaluated separately. At this stage, force-displacement curves (F-Δ) for all components are obtained. Later on, when all the components are already defined the mechanical behaviour of the joint can be determined by assembling the contribution of each basic component. As the result of the component method application moment resistance, rotational stiffness and rotation capacity of the joint are derived.

Shortly, the component method can be described in three steps:

- Identification of components,
- Characterisation force-displacement curves (F-Δ) of all components,
- Moment-rotation characteristic (M-ϕ) of the joint by assembling of components.

- **Identification of components**

In the frame of component method each part of a joint, i.e. each basic component, is represented as a extensional spring (Figure 2.19).

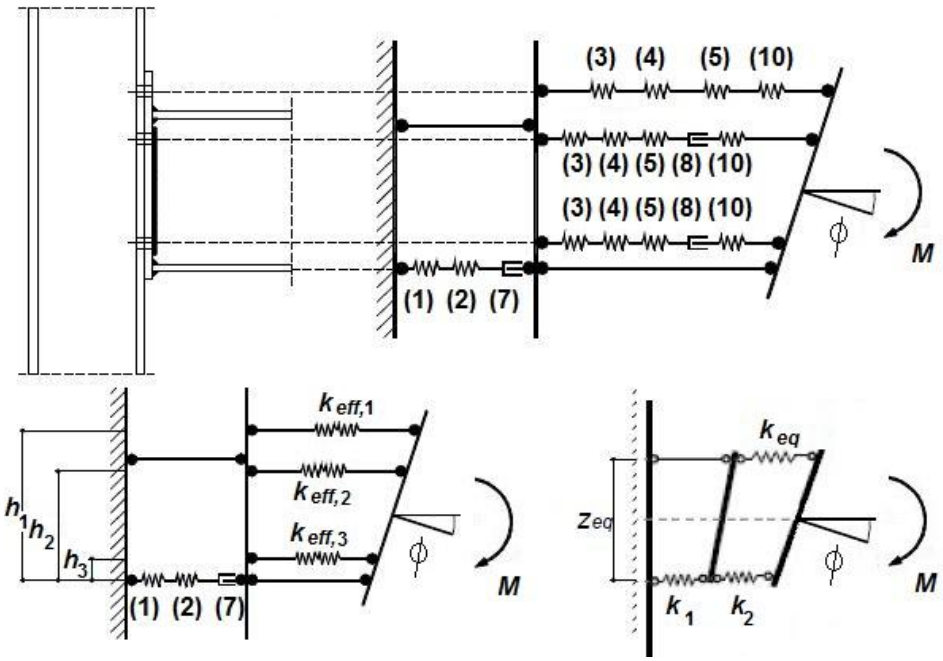

Figure 2.19 Example of spring model of a one-sided bolted beam-to-column connection.

In the Figure 2.19 each spring represents the behavior of one component:

k_1 column web panel in shear,

k_2 column web in compression,

k_3 column web in tension,

k_4 column flange in bending,

k_5 end-plate in bending,

k_7 beam flange and web in compression,

k_8 beam web in tension,

k_{10} bolts in tension.

As it is shown, springs k_1, k_2 and k_7 work in series while three rows of springs k_3, k_4, k_5, k_8 and k_{10} work in parallel. The effect of springs sequence is depicted in Figure 2.20.

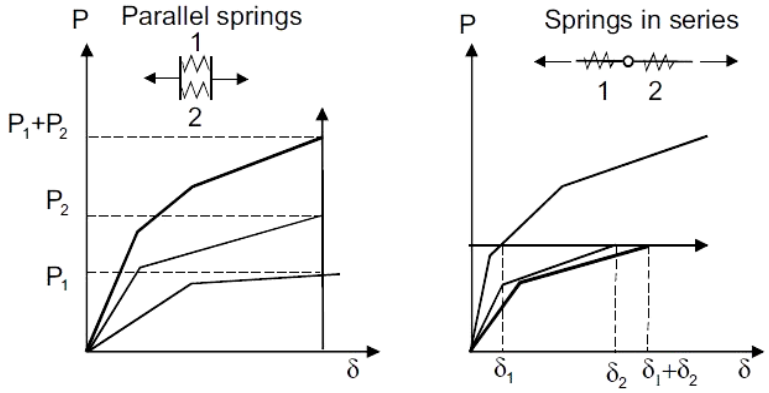

Figure 2.20 Influence of spring sequence on a joint behaviour.

$k_{eff,i}$ is the effective stiffness coefficient calculated for springs in series:

$$k_{eff,i} = \frac{1}{\sum_i \frac{1}{k_i}} \tag{2.1}$$

k_{eq} is the equivalent stiffness coefficient calculated for parallel springs:

$$k_{eq} = \frac{\sum_i k_{eff,i} h_r}{z_{eq}} \tag{2.2}$$

where:

h_r the distance from bolt row in tension to the centre line of compressed zone,

z_{eq} the equivalent lever arm,

$$z_{eq} = \frac{\sum_r k_{eff,r} h_r^2}{\sum_r k_{eff,r} h_r} \tag{2.3}$$

EN 1993-1-8 [CEN, 2005] offers a set of clearly stated recommendations which allow to cover a big range of beam-to-column joint types and facilitate the design process.

According to EN 1993-1-8 [CEN, 2005], the joint basic components used for beam-to-column joints are stated in Table 6.1 EN1993-1-8 (Table 2.1) and their properties should be determined according to the rules given in the Standard. Those joint basic components which are out of the Standard may be applied provided their properties are based on tests or analytical and numerical methods supported by tests.

Table 2.1 Basic joint components according to EN 1993-1-8 [CEN, 2005].

№.	Component	Reference to EN 1993-1-8 [CEN, 2005]		
		Design resistance	Stiffness coefficient	Rotation capacity
1	Column web panel in shear	6.2.6.1	6.3.2	6.4.2, 6.4.3
2	Column web in transverse compression	6.2.6.2	6.3.2	6.4.2, 6.4.3
3	Column web in transverse tension	6.2.6.3	6.3.2	6.4.2, 6.4.3
4	Column flange in bending	6.2.6.4	6.3.2	6.4.2, 6.4.3
5	End-plate in bending	6.2.6.5	6.3.2	6.4.2
6	Flange cleat in bending	6.2.6.6	6.3.2	6.4.2
7	Beam or column flange and web in compression	6.2.6.7	6.3.2	*)
8	Beam web in tension	6.2.6.8	6.3.2	*)
9	Plate in tension or compression	EN 1993-1-1	6.3.2	*)
10	Bolts in tension	With column flange: 6.2.6.4 With end plate: 6.2.6.5 With flange cleat:6.2.6.6	6.3.2	6.4.7
11	Bolts in shear	3.6	6.3.2	6.4.2
12	Bolts in bearing (on beam flange, column flange, end-plate or cleat)	3.6	6.3.2	*)
19	Welds	4	6.3.2	*)
*) No information available in this part.				

- **Characterisation force-displacement curves (*F*-Δ) of all components**

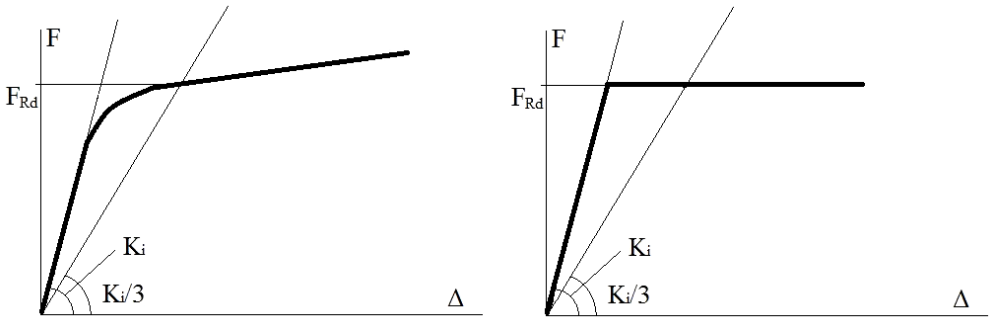

Figure 2.21 Force-displacement curves of a component: actual behaviour and bi-linear simplification.

The stiffness K_i should be evaluated from elastic modulus and stiffness coefficient k_i as follows:

$$K_i = Ek \tag{2.4}$$

The secant stiffness K_i corresponding to resistance equals to stiffness divided by 3 what is suggested by Faella, Piluso and Rizzano [Faella *et al*., 1999].

- **Moment-rotation characteristic (*M*-ϕ) of the joint by assembling of components**

The assembly of each component contribution is based on the distribution of internal forces within the joint. This contribution can be obtained with application of EN 1993-1-8 [CEN, 2005]. Although, stiffness and strength characterisation can be evaluated using numerical simulations by virtue of finite element analysis and/or analytical solution validated by experimental data.

Figure 2.22 Moment-rotational curve of a joint: actual behaviour.

The initial rotational stiffness $S_{j,ini}$ of the bolted beam-to-column joint (Figure 2.19) can be derived by the following expression:

$$S_{j,ini} = \frac{Ez_{eq}^{\ 2}}{\sum_i \frac{1}{k_i}} \tag{2.5}$$

The moment resistance of the welded beam-to-column joint can be obtained as followed:

$$M_{j,Rd} = \min(F_{Rd,i} z_i) \tag{2.6}$$

The moment resistance of the bolted beam-to-column joint (Figure 2.19) can be obtained as followed:

$$M_{j,Rd} = \sum_r h_r F_{tr,Rd} \tag{2.7}$$

if $N_{Ed} \leq 0.05 N_{b,pl,Rd}$

where:

$F_{tr,Rd}$ the effective design tension resistance of bolt row *r*,

h_r the distance from bolt row *r* to the centre of compression,

r the bolt row number,

N_{Ed} the design value of the connected member axial force,

$N_{b,pl,Rd}$ the design plastic resistance of the connected member.

2.3.3. Joint modeling

Joints should be designed in the way which represents the real behaviour as much as it is possible.

There are two main characteristics of each joint: stiffness and resistance. They are discussed in the following paragraphs. Combining these characteristics it's assumed that all joints are divided into three joint models: rigid / full-strength, rigid / partial-strength and pinned. Though, considering economical aspects additional joint models are introduced: semi-rigid / full-strength, semi-rigid / partial-strength.

EN 1993-1-8 [CEN, 2005] offers a simplified identification of joint models as following:

- simple, in which the joint may be assumed not to transmit bending moments (covers pinned model),
- continuous, in which the behaviour of the joint may be assumed to have no effect on the analysis (covers rigid / full-strength model),
- semi-continuous, in which the behaviour of the joint needs to be taken into account in the analysis (covers rigid / partial-strength, semi-rigid / full-strength, semi-rigid / partial-strength models).

According to EN 1993-1-8 [CEN, 2005], a simplified method can be used for one-sided and two-sided joints. A single-sided joint configuration may be modeled as a single joint, and a

double-sided joint configuration may be modeled as two separate but inter-acting joints, one on each side.

In a double-sided beam-to-column joint each joint should be modeled as a separate rotational spring (Figure 2.23). As a consequence, a double-sided beam-to-column joint configuration has two moment-rotation characteristics. The possible influence of the web panel in shear should be taken into account by means of transformation parameters β_1 and β_2 according to Chapter 5.3 of EN 1993-1-8 [CEN, 2005].

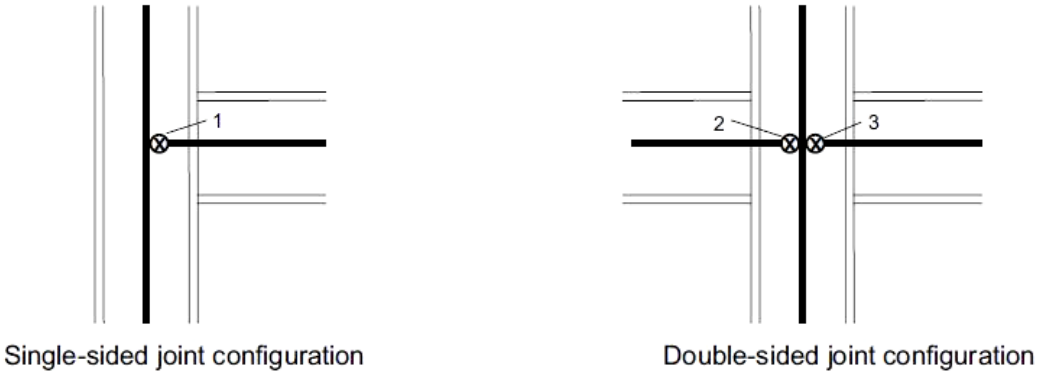

Figure 2.23 Modelling of the joint.

2.3.4. Classification by stiffness

All joint have to be classified by their stiffness as rigid, nominally pinned or semi-rigid. The procedure is accomplished by comparison of initial rotational stiffness of a joint to two boundaries (Figure 2.24). All joints should be capable to accept rotations under design loads, i.e. joints must have sufficient rotation capacity.

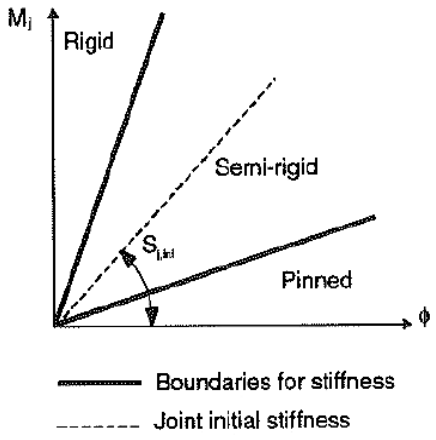

Figure 2.24 Classification by stiffness.

The boundaries are defined in EN 1993-1-8 [CEN, 2005] as following:

- **Boundary conditions for a rigid joint**

$$S_{j,ini} \geq k_b EI_b / L_b \tag{2.8}$$

where:

k_b = 8 for frames where the bracing system reduces the horizontal displacement by at least 80 %,

k_b = 25 for other frames, provided that in every storey $K_b / K_c \geq 0.1$.

- **Boundary conditions for a nominally pinned joint**

$$S_{j,ini} \leq 0.5EI_b / L_b \tag{2.9}$$

- **Boundary conditions for a semi-rigid joint**

All joints not satisfying these boundaries are classified as semi-rigid.

2.3.5. Classification by strength

A joint may be classified as full-strength, nominally pinned or partial strength by comparison of its design moment resistance to resistance for full-strength and pinned boundaries (Figure 2.25).

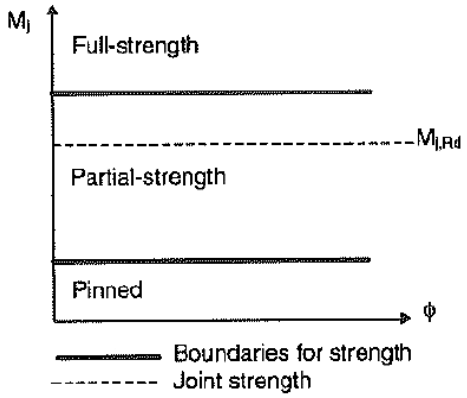

Figure 2.25 Classification by strength.

- **Full-strength joints**

The joint design resistance should be not less than the design moment resistances of the members that it connects as it is stated in EN 1993-1-8 [CEN, 2005] (Figure 2.26).

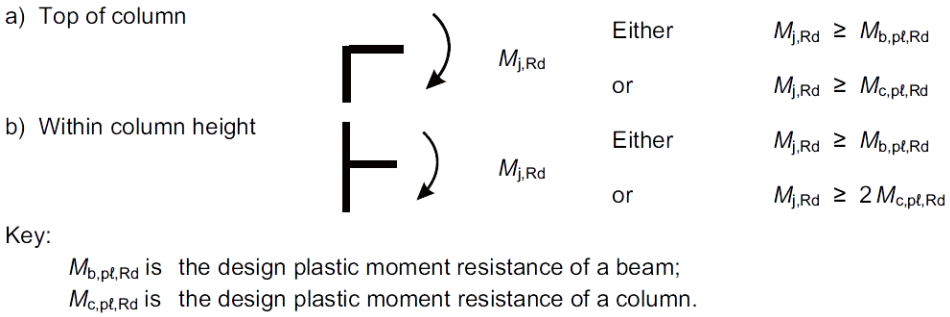

Figure 2.26 Full-strength joints.

- **Nominally pinned joints**

A joint may be classified as nominally pinned if its design moment resistance $M_{j,Rd}$ is not greater than 0,25 times the design moment resistance required for a full-strength joint, provided that it also has sufficient rotation capacity EN 1993-1-8 [CEN, 2005].

- **Partial strength joints**

All joints not satisfying these boundaries are considered as partial strength.

2.3.6. Joint idealisation

EN 1993-1-8 [CEN, 2005] states that for an elastic-plastic analysis non-linear moment-rotation curve can be simplified in order to facilitate the design procedure of a joint. The simplest possible idealisation is the bi-linear model which can be adopted considering the elastic-perfectly plastic relationship (Figure 2.27) provided that the approximate curve lies wholly below the design moment-rotation characteristic. The difference between the original curve and the yield plateau of the idealisation is explained by neglecting of strain hardening effects and possible membrane effects.

As a simplification, the joint rotational stiffness may be taken as $S_{j,ini} / \eta$ for all values up to reaching the design moment resistance $M_{j,Rd}$, where η is taken according to Table 5.2 of EN 1993-1-8 [CEN, 2005].

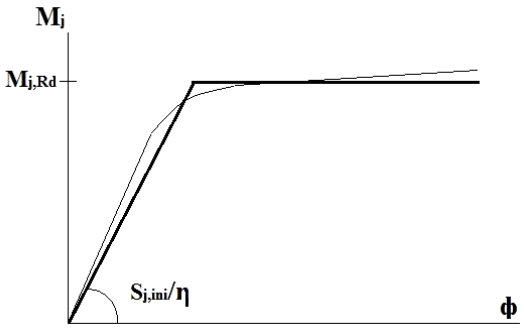

Figure 2.27 Bi-linear moment-rotation curve idealisation.

3.EXPERIMENTAL WORK

3.1. Introduction

The present chapter is dedicated to the description of the beam-to-RHS column joint and also to the detailed study of the compressed components of the joint. The compressed components of the joint are investigated by experimental testing procedure and numerical analysis.

3.2. The beam-to-RHS column joint

The studied joint from the structural point of view is the beam-to-column connection under the monotonic load. The column is represented by a rectangular hollow section and the beam is represented by an I-section profile. Connection is implemented with a usage of two U-sections stiffened by the vertical plate, welded end plates and connected by bolts as it is depicted in the Figure 3.1.

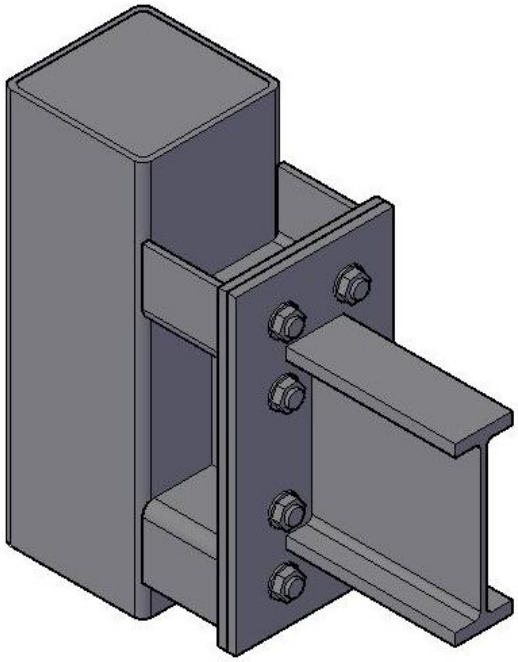

Figure 3.1 3D view of the beam-to-RHC column joint.

As it was already discussed previously, the description of the joint behaviour should be carried out based on the component method. All the recommendations for joint design based on the behaviour of basic joint components are presented in EN 1993-1-8 [CEN, 2005]. Eurocode covers the most of the joint components but still there are several components which are not highlighted in Eurocode. The conclusion about their behaviour can be evaluated based on a complex of experimental data and numerical simulations which are considered to consist of several parts as listed below:

- Study of compressed components of the joint,
- Study of tensile components of the joint,
- Study of the joint behaviour.

The study of the compressed components of the joint is followed in the next chapters along with the further comparison of FE models to experimental data in order to analyse their mechanical behaviour and evaluate a sequence of force-displacement response of models with different geometry through the parametric study.

3.3. Components of the joint

In this chapter, the description of the basic joint components and their classification are provided. As it was highlighted previously, in order to avoid the implementation of demanding non-linear finite element analysis in the determination of the joint moment-rotation response, there is an easier approach based on so-called component method.

The component method allows to model a joint based on already existing knowledge of basic joint components behaviour. Basic components of the particular joint are presented in the Figure 3.2. Subjected to a negative bending moment, basic components of the joint form three groups as followed.

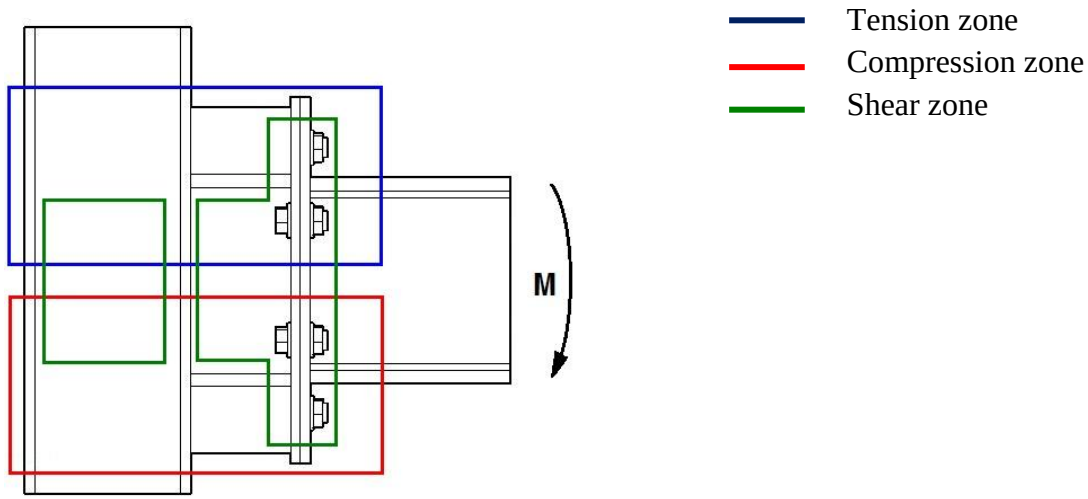

Figure 3.2 Beam-to-RHS column joint basic components.

- Tension zone:
  - Column web in tension,
  - U-section web in tension,
  - U-section flanges in tension,
  - End plate in bending,

- Beam web in tension,
- Bolts in tension.

- Compression zone:
  - Column web in compression,
  - U-section web in compression,
  - U-section flange in compression,
  - Beam flange and web in compression.
- Shear zone:
  - Column web panel in shear,
  - Vertical stiffener web in shear.
- Welds.
- Bolts in bearing.
- Bolts in shear.

There is a number of basic joint components which behaviour is already defined by a convenient procedure stated in EN 1993-1-8 [CEN, 2005]. Although, some of them are new components. All the components are listed in the Table 3.1 with the reference to the appropriate calculation recommendations given in the Standard.

Table 3.1 Definition of the main parameters of basic joint components.

Component	Reference to EN 1993-1-8 [CEN, 2005]		
	Design resistance	Stiffness coefficient	Note
Tension zone			
Column web in tension	6.2.6.3	6.3.2	Note 1
U-section web in tension	--	--	Note 2
U-section flanges in tension	--	--	Note 2
End plate in bending	6.2.6.5	6.3.2	Note 3
Beam web in tension	6.2.6.8	Note 4	
Bolts in tension	6.2.6.5	6.3.2	
Compression zone			
Column web in compression	6.2.6.2	6.3.2	Note 1
U-section web in compression	--	--	Note 2
U-section flange in compression	--	--	Note 2
Beam flange and web in compression	6.2.6.7	Note 4	

Component	Reference to EN 1993-1-8 [CEN, 2005]		
	Design resistance	Stiffness coefficient	Note
Shear zone			
Column web panel in shear	6.2.6.1	6.3.2	
Vertical stiffener web in shear	6.2.6.1	6.3.2	Note 1
Welds			
Welds	4	Note 4	
Bolts			
Bolts in shear	3.6	6.3.2	
Bolts in bearing	3.6	6.3.2	

Note 1: Due to the specific joint configuration the design resistance and stiffness coefficient should be calculated taking into account adapted geometrical parameters.

Note 2: Currently, there is no available data provided for the component, thus it should be obtained by numerical analysis and experimental results.

Note 3: Although the component is already defined in EN 1993-1-8 [CEN, 2005], it can be adopted in accordance with the new joint configuration.

Note 4: According to EN 1993-1-8 [CEN, 2005], beam flange and web in compression, beam web in tension and welds are omitted as basic joint components when calculating the rotational stiffness of a joint.

In order to evaluate an approach for the new basic component, namely U-section web and flange in compression, the thesis presents the numerical analysis is performed and validated by comparing to experimental data.

3.4. Experimental specimen description

The part of the joint which represents the compressed zone of the beam-to-RHS column joint (Figure 3.3) is studied in details in the following chapters. In the frame of the current work, the main objective of the compressed component is the behaviour of the set of U-sections.

In order to provide a correct distribution of stresses and deformations in the experimental specimens the compressed component of the beam-to-RHS column joint was doubled symmetrically.

Four specimens were tested under the monotonic compression load on the compression testing machine up to the failure when the applied load stops increasing. The load was applied through the bottom platform. The bearing face of the top bearing block was adjusted horizontally to provide as even distribution of the applied load as it is possible.

As it is depicted in the Figure 3.3, the experimental specimen consists of five details. Description of each detail follows.

Position 1: two U-sections are welded to the end plate, base plates and to the vertical stiffener.

Position 2: Vertical stiffener is located between U-sections in order to provide additional stiffness to the specimen and avoid excessive deformation of the U-section web.

Position 3: End plate is solid without bolt holes as a simplification in terms of fabrication. Such a simplification is assumed considering the specimen as a subject of the compressive load only.

Position 4: Loading plates are welded to the end plate. Loading plates reproduce the loaded area in the compression zone of the joint.

Position 5: Base plates are welded to U-sections and represent the column wall of the joint. In order to not over restrict vertical deformation of U-sections, there are cuts executed in the base plates. The cuts are carried out due to the assumption to neglect the support of the U-section along the bottom face of the channel web. Such an assumption is possible due to low stiffness of the column wall. Base plate cuts are depicted in details in the Figure 3.4.

All welds are according to the sketch pictured in the Figure 3.4.

U-sections are implemented by steel hollow sections cut lengthwise.

The joint details are performed by steel grade S355, U-sections are according to EN 10210-1 [CEN, 2006], all the plates are according to EN 10025-2 [CEN, 2004].

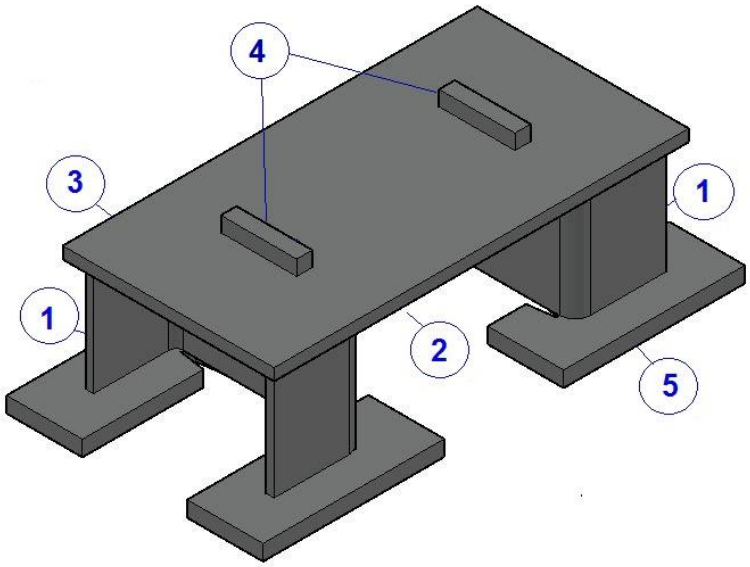

1 U-section

2 Vertical stiffener

3 End plate

4 Loading plate

5 Base plate

Figure 3.3 3D view of the symmetrical specimen of the compressed component of the joint.

The sketch of the specimens is pictured in Figure 3.4. There is a number of variable parameters what aims to investigate the behaviour of the specimens in a wider range.

Variable parameters are as followed:

- U-section thickness (t),
- U-section height (h),
- U-section flange width (B),
- Loading plate length (L_{load}).

Particular values of variable parameters of the four experimental specimens are presented in the Table 3.2.

Table 3.2 Dimensioning of compressed zone experimental specimens.

Test №	Test name	U-section parameters			Loading plate
		h, [mm]	B, [mm]	t, [mm]	L_{load}, [mm]
Test 01	Test01_2U_h100b80t8L100	100	80	8	100
Test 02	Test02_2U_h100b80t8L210				210
Test 03	Test03_2U_h150b120t10L100	150	120	10	100
Test 04	Test04_2U_h150b120t10L210				210

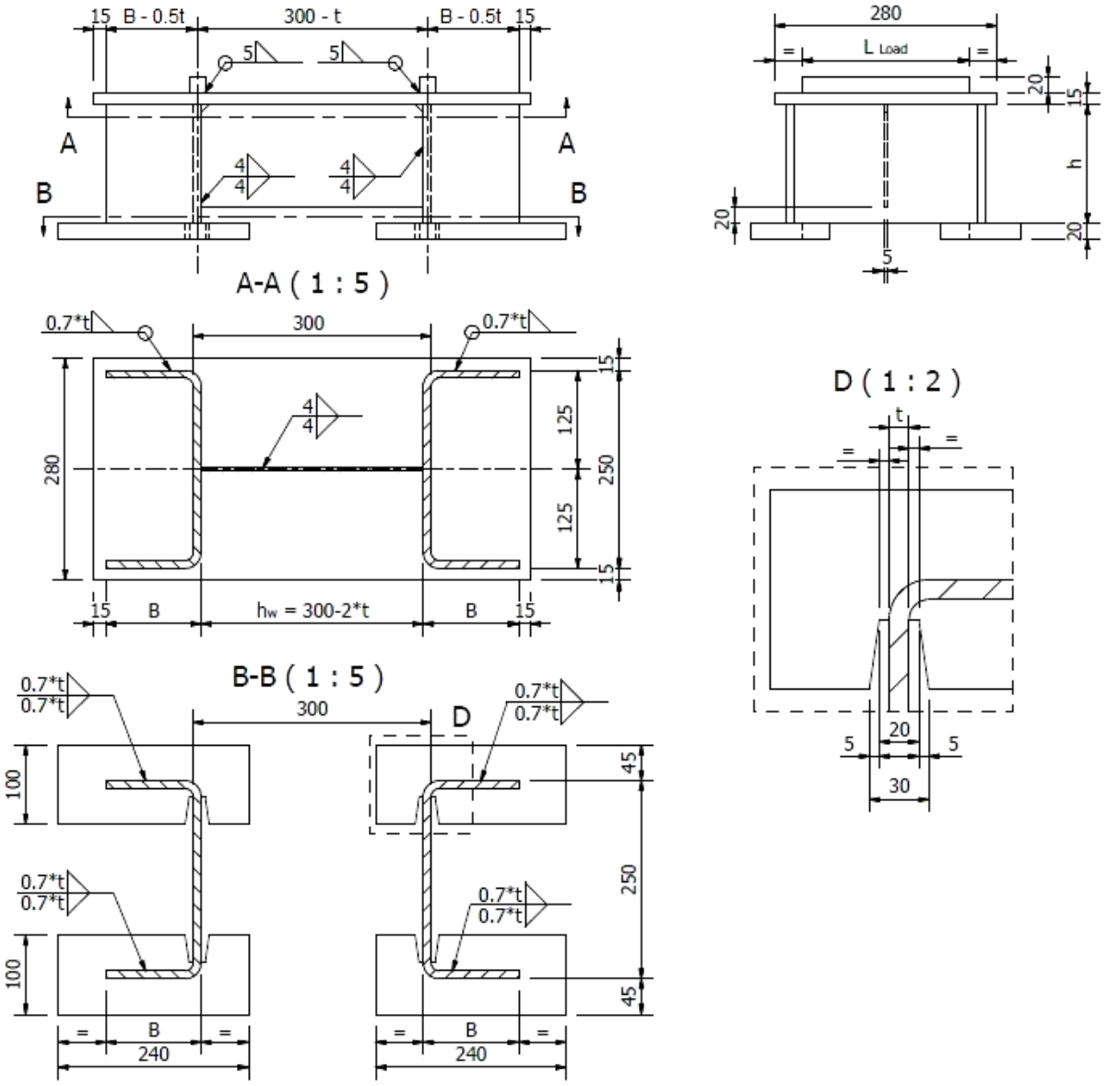

Figure 3.4 The sketch of experimental specimens.

The output of experiments consists of the following information:

- Force-displacement response,
- Force-strain response.

Vertical displacements were measured through four transducers. Two of them were placed on the bottom elevation platform. The final displacement of the elevation platform is an average of two results. Other two transducers were connected to specimens' end-plate and measured vertical displacement corresponding to the load application point through the angle of rotation of the end plate. The experimental set-up is depicted in the Figure 3.5.

The applied force was measured through the transducer at the load application point.

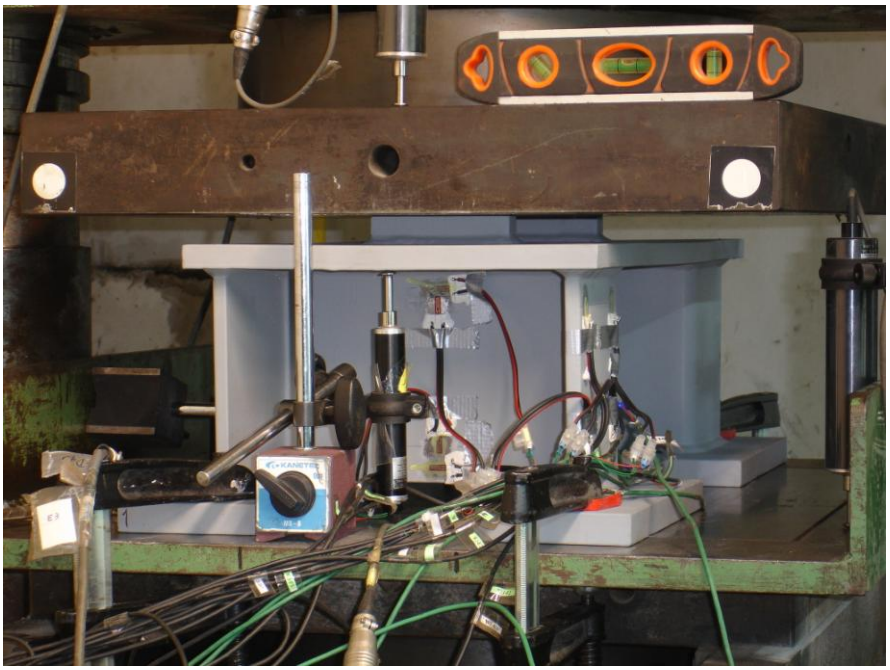

Figure 3.5 The test set-up before the initiation of the loading.

The force-strain response was obtained for 14 points, 10 of them were located on the U-section and 4 of them were on the vertical stiffener. Strains were evaluated by strain gauges located in each point as it is depicted in the Figure 3.6 (all dimensions are in mm).

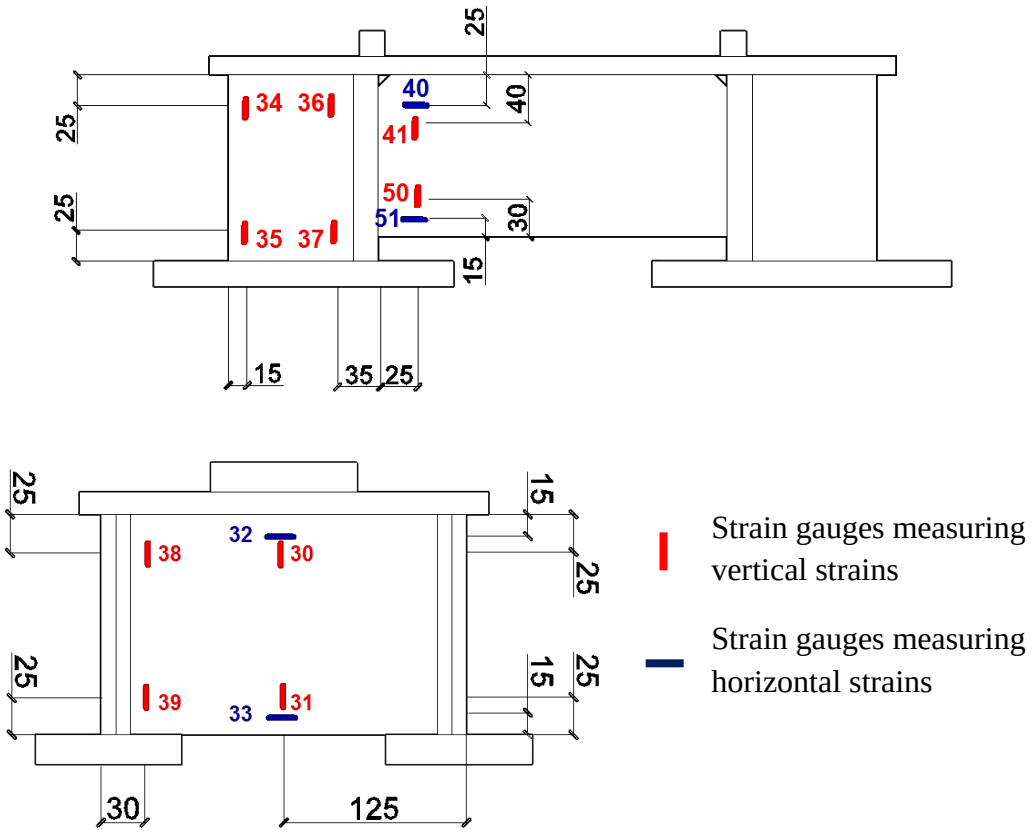

Figure 3.6 Location of strain gauges on the testing specimen.

3.5. Experimental output

As it was previously highlighted, the experimental output includes the information about the force-displacement response. There are two force - displacement curves obtained by each experiment. The curve *ΔTest№_Platform* is corresponding to data obtained by the average value of the vertical displacement of the bottom platform. The curve *ΔTest№_Load point* provides data of the vertical displacement at the load application point. Both of curves are shown in the Figure 3.7 to Figure 3.10 including the graphical image of stiffness and secant stiffness. Resistance and stiffness coefficient are presented in the Table 3.3.

All the curves are translated to the origin. The translation was done due to initial adjustments at the first stage of the load application.

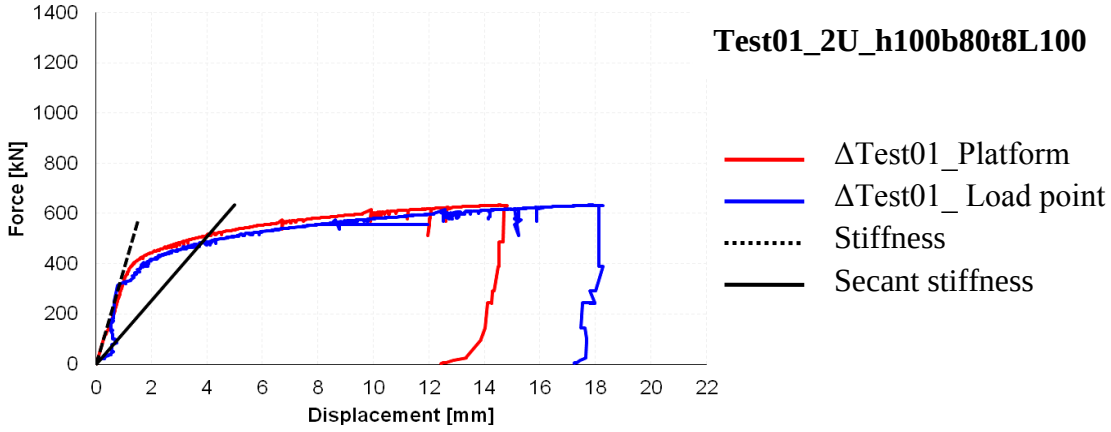

Figure 3.7 Experimental force-displacement curves of Test01 translated to the origin.

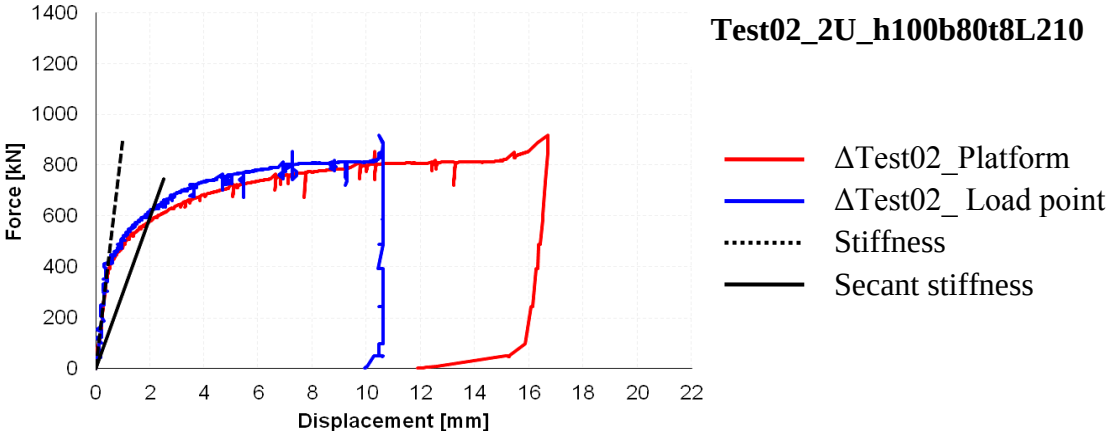

Figure 3.8 Experimental force-displacement curves of Test02 translated to the origin.

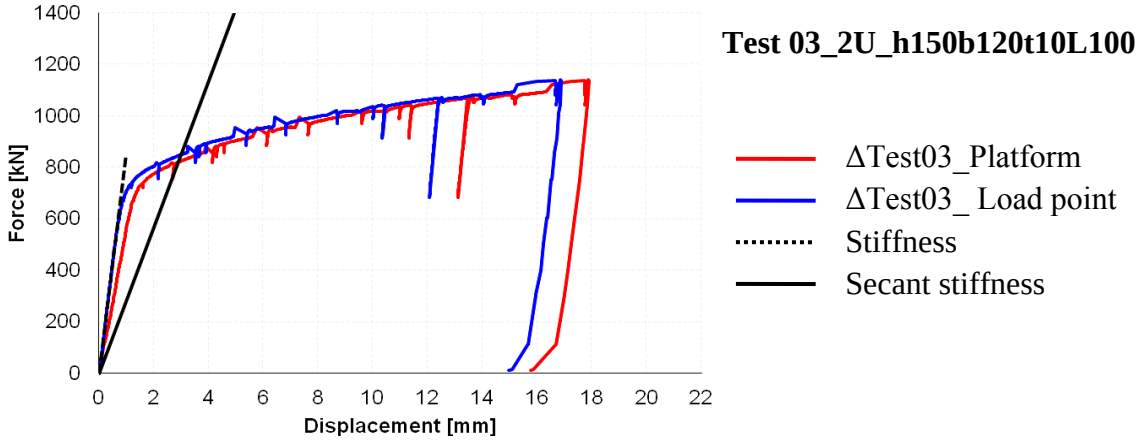

Figure 3.9 Experimental force-displacement curves of Test03 translated to the origin.

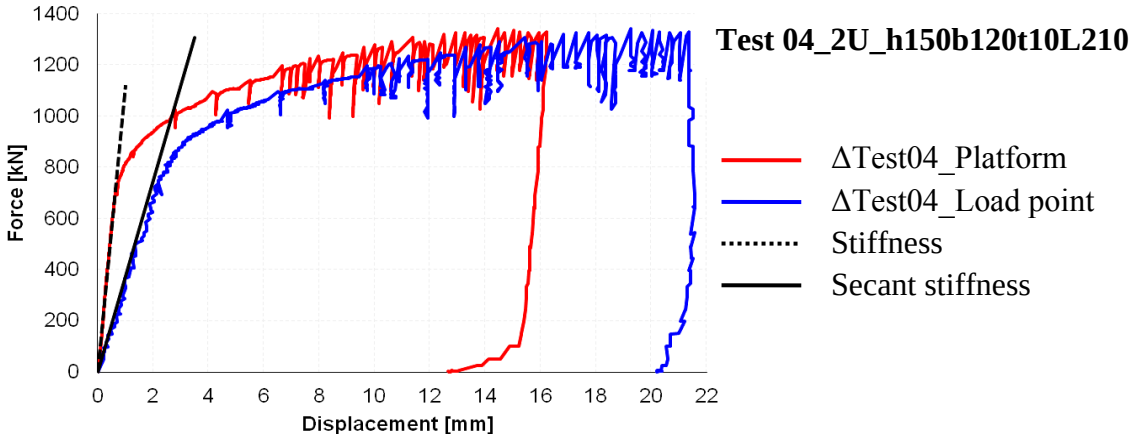

Figure 3.10 Experimental force-displacement curves of Test04 translated to the origin.

Table 3.3 Experimental resistance and stiffness coefficient.

Test №	Test name	Resistance	Stiffness coefficient, *k*		
			Platform	Load point	Final
		[kN]	[mm]	[mm]	[mm]
Test 01	Test01_2U_h100b80t8L100	510.50	1.58	1.12	1.58
Test 02	Test02_2U_h100b80t8L210	611.79	4.06	4.31	4.31
Test 03	Test03_2U_h150b120t10L100	837.42	2.72	4.16	4.16
Test 04	Test04_2U_h150b120t10L210	978.66	5.49	1.62	5.49

Analysing values of the stiffness coefficients listed above one may notice that there is a significant difference between two curves obtained for Test03 (2.72 mm and 4.16 mm) and Test04 (5.49 mm and 1.62 mm). Obviously, such a difference cannot be veritable and might be caused by equipment problems during the testing.

Furthermore, both of values of stiffness coefficient obtained for the Test01 (1.58 mm and 1.12 mm) are suspected to be lower than expected as they are not consistent to those values for other three tests. It can be better understood onwards by comparing to the numerical solution.

Thus, for the purpose of the validation of the numerical model the most reliable values were chosen. They are marked as "Final stiffness coefficient" in the Table 3.3. Hereinafter, just the value of the "Final stiffness coefficient" will be used in the present thesis as the experimental stiffness coefficient.

Force - strain curves obtained by experimental tests are presented in the Chapter 4.4 "Validation of the model" along with the comparison to the numerical results.

The deformed shape of the tested specimens may be observed in the Figure 3.8.

a) Front view.

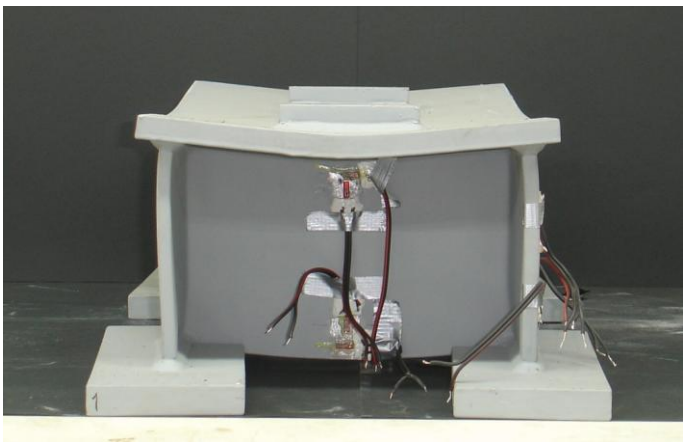

b) Side view.

Figure 3.11 Deformed shape of the tested specimen Test03.

4.NUMERICAL SIMULATIONS

4.1. Overview

In the frame of this thesis, numerical simulation is carried out using *DS Simulia Abaqus* software. Overall, there are 108 numerical models which were used in order to obtain a clear understanding of the compressed zone behaviour through the parametric study. Four of these models are implemented repeating the geometry of experimental testing samples for calibration of the modeling assumptions.

4.2. Finite element model description

- **Material modeling**

All elements of the joint are presented by steel with elastic-plastic material behaviour. Elastic properties of steel are introduced considering isotropic linear elastic material behaviour. Plastic properties are entered by the application of the plasticity model based on Mises yield surface considering isotropic hardening.

When defining the plasticity in *Abaqus*, true stress and true strain values should be used.

Material's mechanical response is based on the results of tensile tests of steel extracted from experimental samples. Experimental data provides an engineering stress-strain curve which gives the information about nominal values of stress and strain. Thus, in the plastic range, obtained values should be converted to true stress and true strain using the following formulas:

$$\sigma_{true} = \sigma_{nom} (1+ \varepsilon_{nom}) \tag{4.1}$$

$$\varepsilon_{true} = \ln(1+ \varepsilon_{nom}) \tag{4.2}$$

where:

ε_{nom} is the nominal strain,

ε_{true} is the true strain,

σ_{nom} is the nominal stress,

σ_{true} is the true stress.

Then, values of true strain should be also converted into plastic strain in the plastic range of the stress-strain curve. These values are obtain using the formula below:

$$\varepsilon_{pl} = \varepsilon_{true} - \sigma_{true} / E \tag{4.3}$$

Taking into account the stress and strain conversion, steel properties used as the input to finite element analysis are as it follows in the Table 4.1.

Table 4.1 Steel properties used in FEA.

Steel name	Modulus of elasticity [N/mm^2]	Poisson's ratio	Plastic range	Definition
Steel Plate	210674	0.3	Figure 4.1	All steel plates
Steel 1	207616	0.3	Figure 4.1	U-sections of thickness 6 mm and 8 mm
Steel 2	204200	0.3	Figure 4.1	U-sections of thickness 10 mm

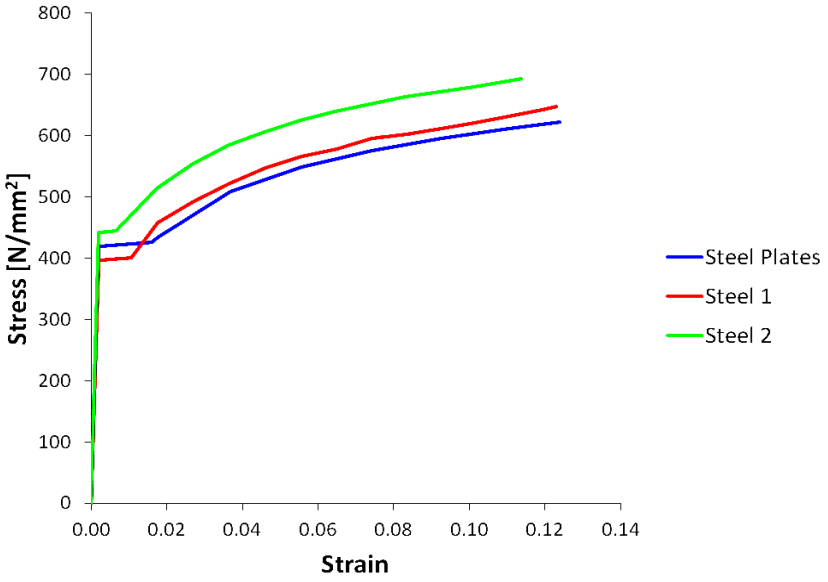

Figure 4.1 Stress - strain response of steel S355.

- **Model description**

Models are implemented using 3D solid deformable elements (continuum elements).

Different parts of the model are connected together by their surfaces using tie constraints. This type of constraint provides that the motion of a point of one surface totally repeats the motion of a point belonging to another surface.

All the welds are considered in the analysis by their geometry only. The post-welding effects of heating during the welding process are neglected.

- **Finite element mesh**

Type of mesh is C3D8R which is hexahedral 8-node brick element with reduced integration. This type of finite element belongs to three-dimensional continuum (solid) elements and has tree translational degrees of freedom in each node [Abaqus user's manual, 2007].

The number of finite elements may strongly affect output results. This is the reason why the mesh convergence analysis is done. Detailed information about the mesh convergence study is presented in the Chapter 4.3 "Mesh convergence analysis" of the thesis.

- **Boundary conditions and loading**

Load application point is connected to top faces of loading plates through continuum distribution coupling constraint which couples translational and rotational degrees of freedom of connected surfaces to the motion of the point. It allows to simulate real boundary conditions of the loading plates during experiments.

The load is introduced to the model as the vertical displacement of 15 mm. It is applied to the load application point as it is shown in the Figure 4.2. From this point the displacement translates to the top faces of the loading plates.

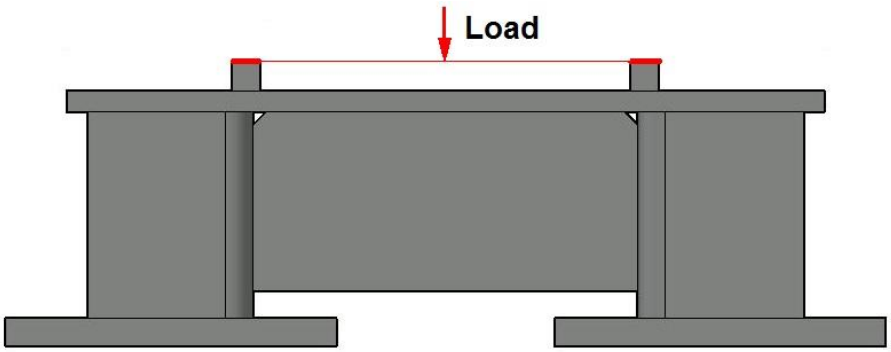

Figure 4.2 Load application to the numerical model.

Boundary conditions are introduced to the model through the limitation of translation degrees of freedom of the base plates along *X*, *Y* and *Z* directions.

- **Analysis type and imperfections**

The numerical analysis is done considering the geometrical and material nonlinearity. Another source of nonlinearity arises from material non-linear properties which is already included into analysis.

Geometrical imperfections are omitted in the numerical models as it is assumed that the influence of those imperfections is negligible due to small dimensions of the compressed components.

- **Numerical analysis output**

As the direct result of the numerical analysis, displacements, strains and corresponding applied force are obtained.

Applied vertical force RF2 is measured in the load application point. The vertical displacement U2 is measured in the same point as it describes the total displacement of the steel joint. Logarithmic strains LE11 (along *X* axis), LE22 (along *Z* axis) and LE33 (along *Y* axis) are measured in each point corresponding to the position of strain gauges during the testing.

As the indirect result, resistance and stiffness coefficient of compressed component models are obtained. Stiffness coefficient is evaluated from the relation of stiffness to elastic modulus. The resistance is obtained through the secant stiffness which equals to stiffness divided by 3 what is suggested by Faella, Piluso and Rizzano [Faella *et al*., 1999] as it was previously highlighted.

4.3. Mesh convergence analysis

In this clause the mesh convergence study of the model Model 03 corresponding to the test Test03_2U_h150b120t10L100 is presented.

In the frame of mesh analysis four types of meshing were compared. The basic parameters of choosing the mesh type in the present study are stiffness coefficient and resistance.

The first model contains the course mesh including 2 elements across the U-section thickness. The second model contains 3 elements across the U-section thickness. The third model is meshed differently in horizontal and vertical directions (3 elements across the U-section thickness). It was assumed to check if the increased number of finite elements along the load direction brings more accurate result. The fourth model has the finest mesh including 4 elements across the U-section thickness. For obtaining the better image of mesh types their sketches are followed (Figure 4.3 to Figure 4.6).

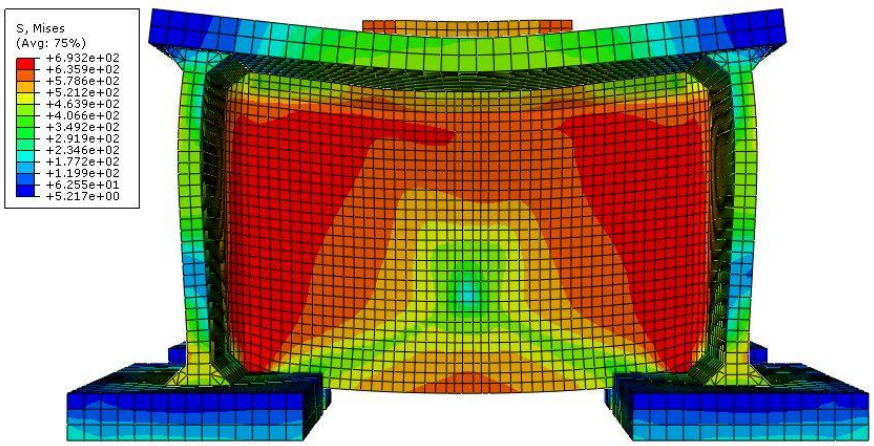

Figure 4.3 Model 03. Mesh 1 (2 finite elements across the U-section thickness).

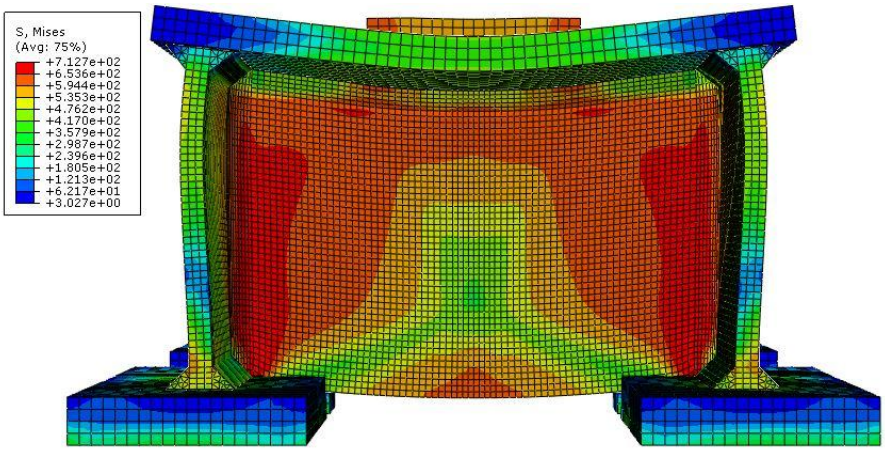

Figure 4.4 Model 03. Mesh 2 (3 finite elements across the U-section thickness).

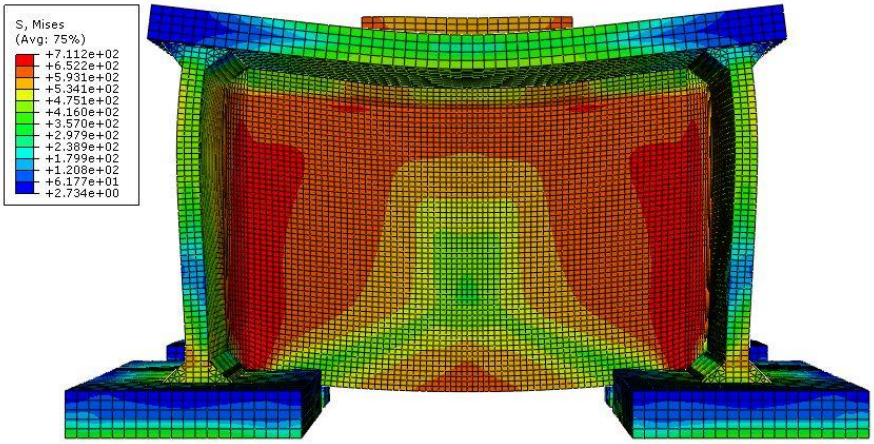

Figure 4.5 Model 03. Mesh 3 (3 finite elements across the U-section thickness).

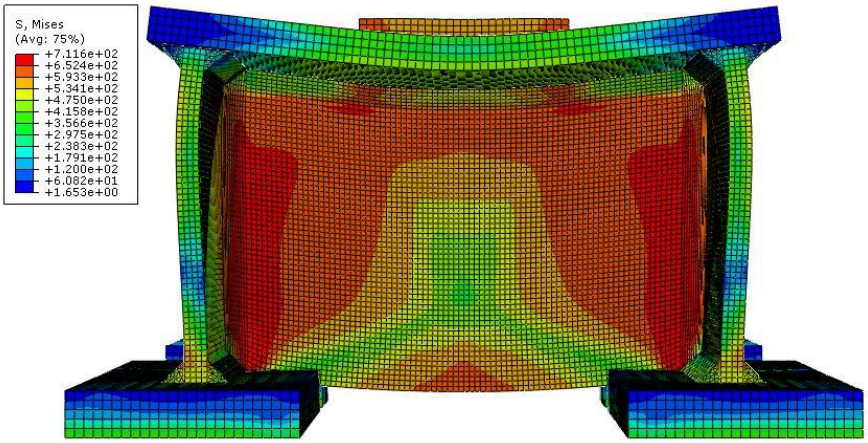

Figure 4.6 Model 03. Mesh 4 (4 finite elements across the U-section thickness).

As it is seen from the Table 4.2, Mesh 1 gives rough results, considering Warning 1 which states that strain increment has exceeded the strain cause to first yield in a number of points. In practice it means that strain evaluation is failed for those points which leads to unreliable results. It can be observed on the Figure 4.3 that numerical problems during the analysis caused non-symmetrical unnatural stress distribution. Mesh 3 gives too high difference of stiffness coefficient which crosses it out of consideration. Mesh 2 and Mesh 4 provides very

similar results of stiffness coefficient and resistance. Actually, the difference of results of Mesh 2 and Mesh 4 is negligible. Figure 4.4 and Figure 4.6 show that the stress distribution is resembling as well. Thus, taking into account the time of calculation, Mesh 2 is chosen for the further analysis.

Table 4.2 The mesh convergence analysis of Model 03.

Mesh	Number of elements	Calculation time	Warnings	$F_{Rd,FEM}$	$F_{Rd,Test}$	ΔF_{Rd}	k_{FEM}	k_{Test}	Δk
				[kN]	[kN]	%	[mm]	[mm]	%
Mesh 1	27667	0 h 20 m	Warning 1	948.62	837.42	11.72	5.05	4.16	17.68
Mesh 2	106205	0 h 40 m	-	973.39		13.97	4.93		15.62
Mesh 3	135841	1 h 10 m	-	965.46		13.26	5.24		20.63
Mesh 4	256149	3 h 10 m	-	972.47		13.89	4.93		15.67

The force to displacement relation can be observed on the Figure 4.7 which shows models with different meshing as well as experimental results of Test03_2U_h150b120t10L100. Two experimental curves are highlighted in the Chapter 3.5 "Experimental output" of the present thesis.

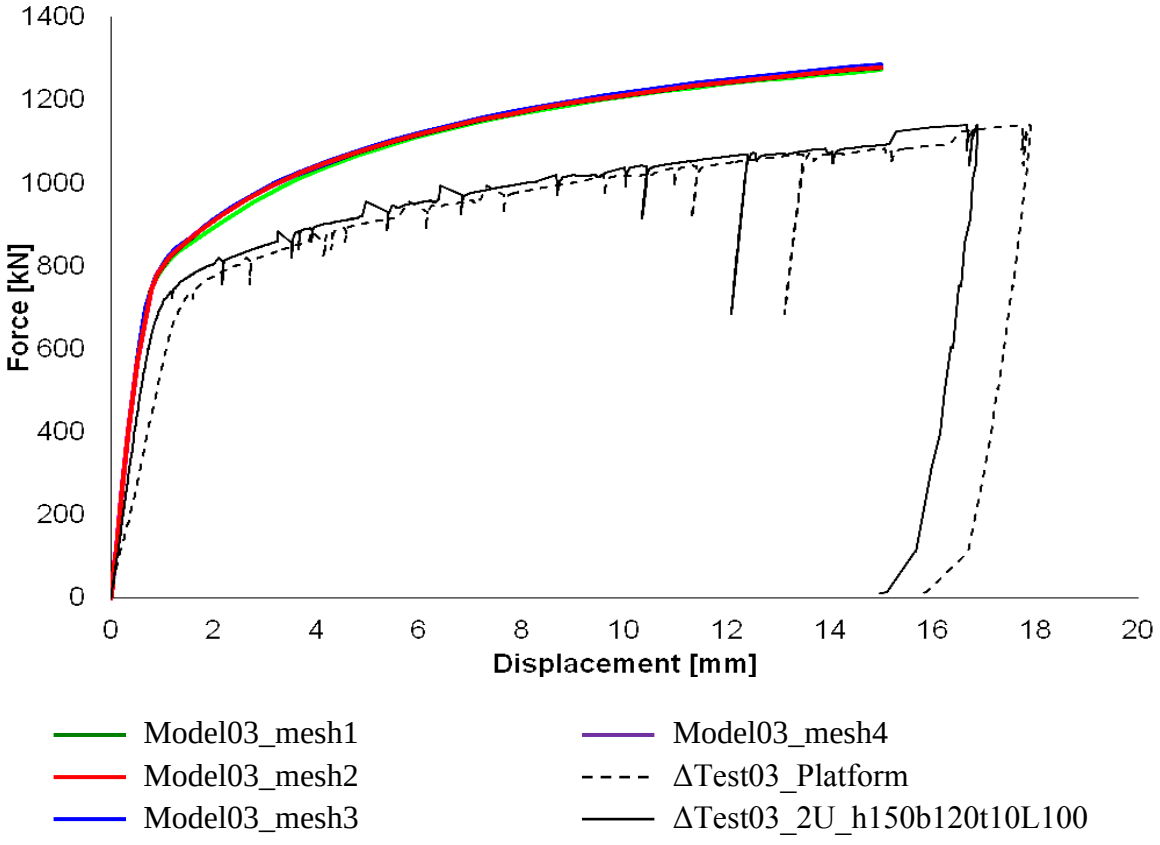

Figure 4.7 Force - displacement curves of mesh convergence analysis of Model 03.

4.4. Validation of the model

Validation of the numerical model is done by comparison of the model behaviour with the specimen behaviour observed during experiments. It is implemented by the following characteristics:

- Force - displacement curve,
- Force - strain curve.

The validation process is done for the numerical models corresponding to experimental tests Test01 to Test04. The comparison of the results obtained numerically and experimentally is expressed on force - displacement diagrams (Figure 4.8 to Figure 4.10). Values of resistance and stiffness coefficient are presented in the Table 4.3.

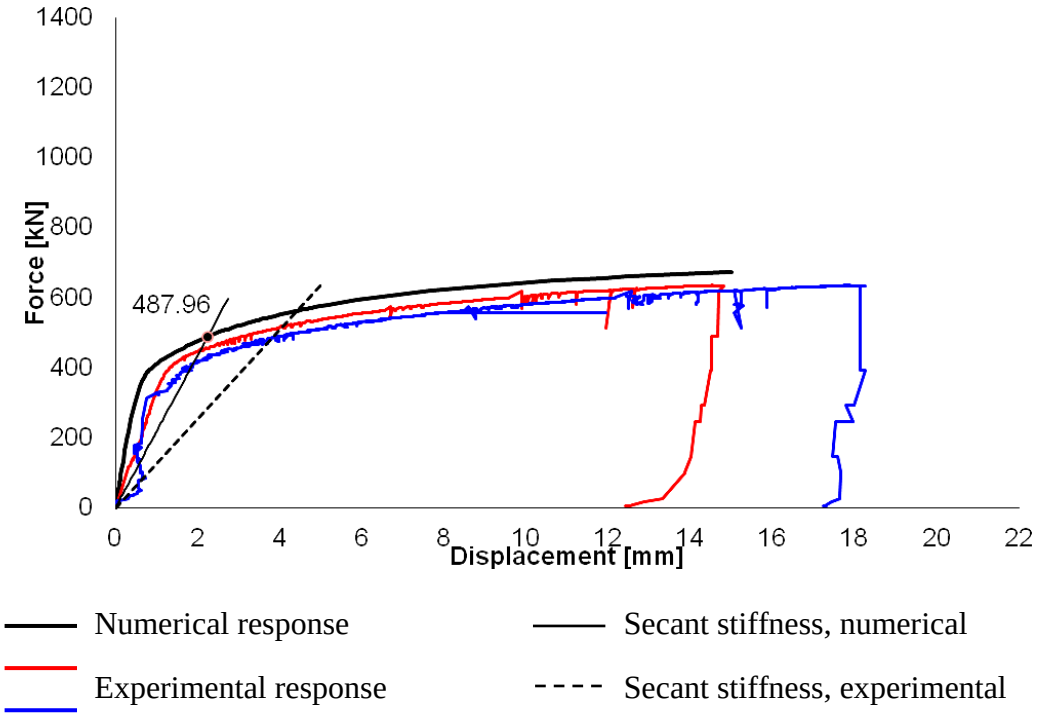

Figure 4.8 Force - displacement response of numerical model Model 01 and experimental data.

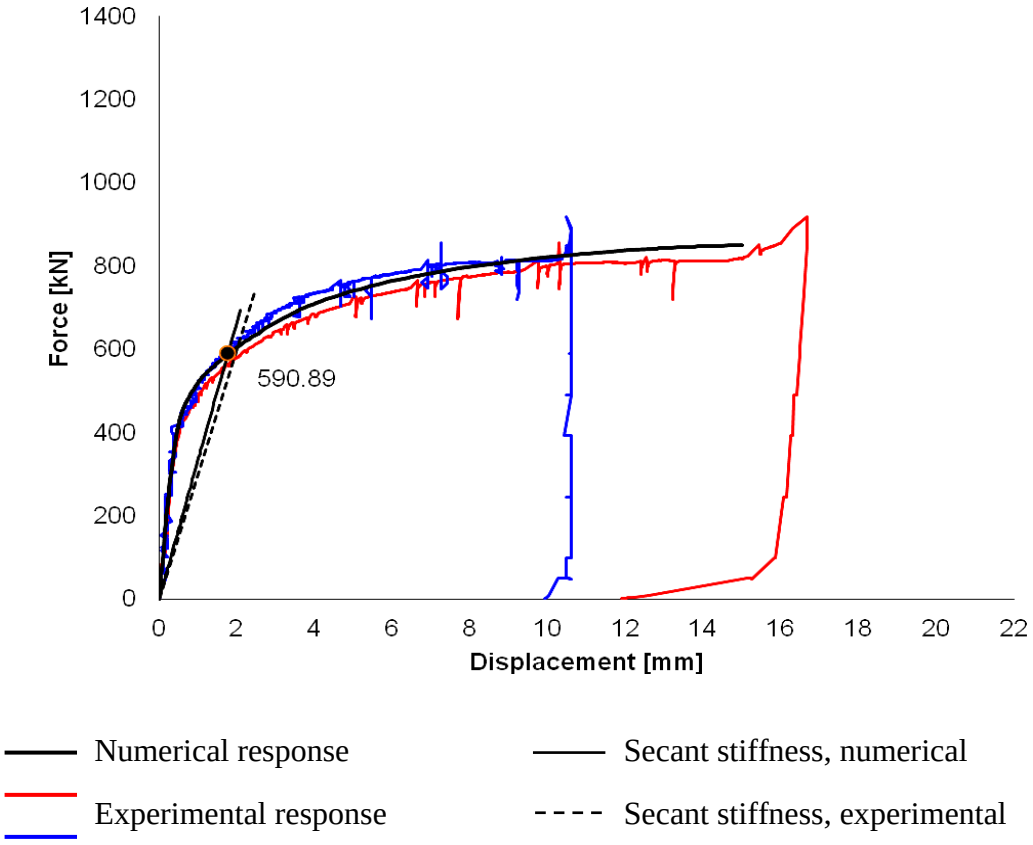

Figure 4.9 Force - displacement response of numerical model Model 02 and experimental data.

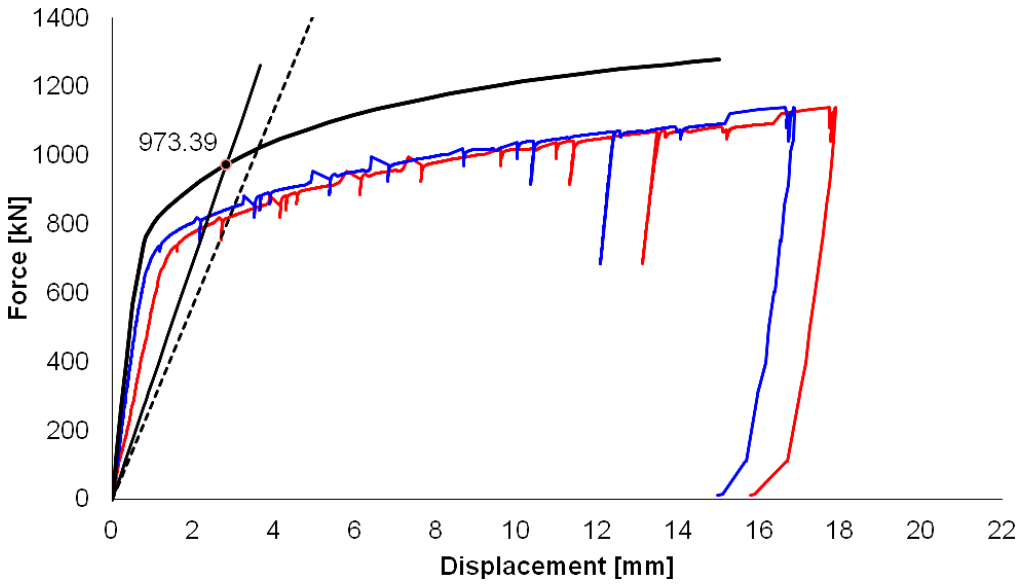

Figure 4.10 Force - displacement response of numerical model Model 03 and experimental data.

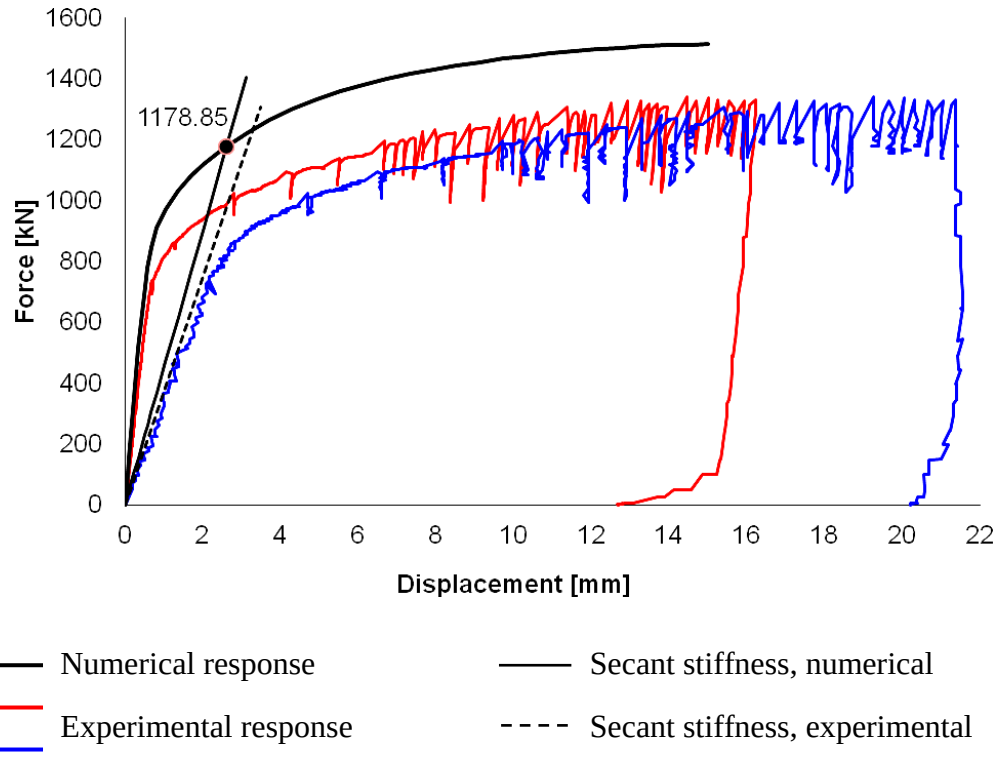

Figure 4.11 Force - displacement response of numerical model Model 04 and experimental data.

Table 4.3 Resistance and stiffness coefficient of numerical models and experimental data.

Model name	Numerical results		Experimental results		Difference	
	Resistance	Stiffness coefficient	Resistance	Stiffness coefficient	Resistance	Stiffness coefficient
	$F_{Rd,FEM}$	k_{FEM}	$F_{Rd,Test}$	k_{Test}	ΔF_{Rd}	Δk
	[kN]	[mm]	[kN]	[mm]	%	%
Model 01	487.96	3.02	510.50	1.58	-4.62	47.72
Model 02	590.89	4.72	611.79	4.31	-3.54	8.61
Model 03	973.40	4.93	837.42	4.16	13.97	15.68
Model 04	1178.85	6.44	978.66	5.49	16.98	14.78

As it can be seen from the Table 4.3, the difference of 47.7% for stiffness coefficient of Model01 can be explained by too low value obtained by the test caused, apparently, by measurement error during the testing implementation of the specimen Test01, as it was previously discussed. This value might be neglected in the validation of numerical models.

Results obtained for Model 02 by numerical analysis and experimental results for Test02 show the error of 3.5% for resistance and 8.6% for stiffness coefficient what is appropriate. Hereby, the model shows a good convergence.

The difference of values of resistance and stiffness coefficient determined for Model 03 and Model 04 is 17% and 15.7% respectively. Comparing to experimental results such a difference is considered to be acceptable.

Thus, the difference between numerical and experimental results is acceptable and numerical models are considered to be validated.

One more subject of interest is the comparison of force versus strain response carried out by numerical analysis and experimentally.

Logarithmic strains are evaluated in points corresponding to those points where strain gauges were placed during experimental tests. Force-strain diagrams for numerical model Model 01 and experimental data obtained for the specimen Test01_2U_h100b80t8L100 are depicted in the Figure 4.12 to Figure 4.25.

Analysing force versus strain curves one may observe that deformations in the top central zone of U-section web remain elastic, i.e. 0.2% in the point 30 (Figure 4.12) and 0.1% in the point 32 (Figure 4.14) while bottom central zone of U-section web experience much higher transverse deformations, i.e. 7% measured in the point 33 (Figure 4.15). U-section web edge zones are the subject of highest level of deformations throughout the U-section, i.e. 7.5% measured in the point 38 (Figure 4.16) and 6.2% in the point 39 (Figure 4.17). U-section flanges experience the higher deformation concentrated in the bottom corner closer to the web, i.e. 2.5% measured in the point 37 (Figure 4.21).

Connecting Web Plate (vertical stiffener) is a subject of low strains through all the height and length, i.e. up to 0.8% measured in the point 40 (Figure 4.24).

Such a mechanical behaviour remains valid for other three models as well but the stress distribution between U-section web and U-section flanges which depends on the length of the loading plate.

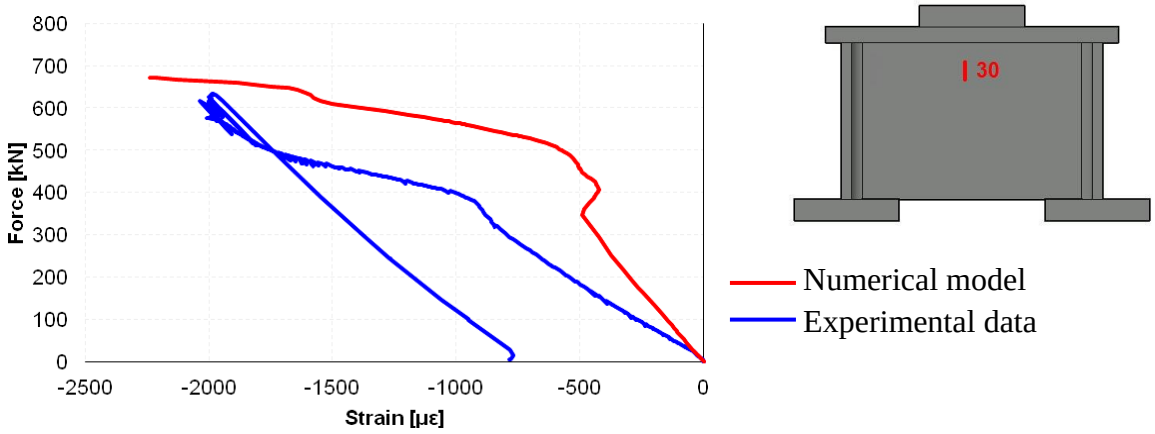

Figure 4.12 Force - strain response of Model 02 and Test02_2U_h100b80t8L210 obtained in the point 30.

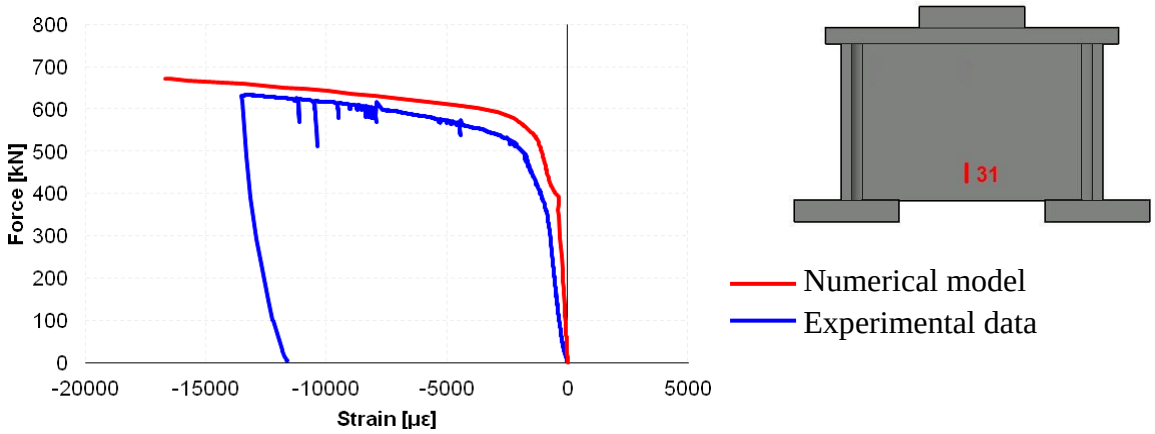

Figure 4.13 Force - strain response of Model 02 and Test02_2U_h100b80t8L210 obtained in the point 31.

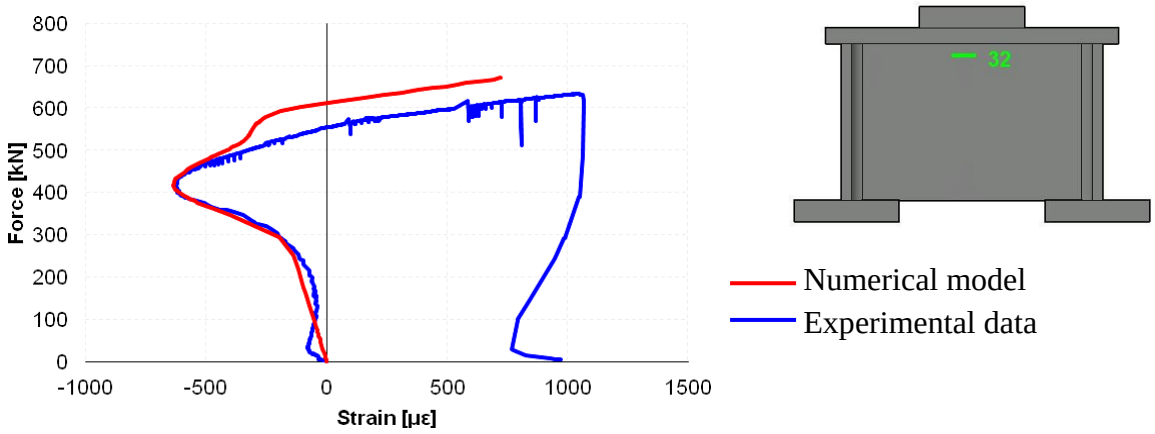

Figure 4.14 Force - strain response of Model 02 and Test02_2U_h100b80t8L210 obtained in the point 32.

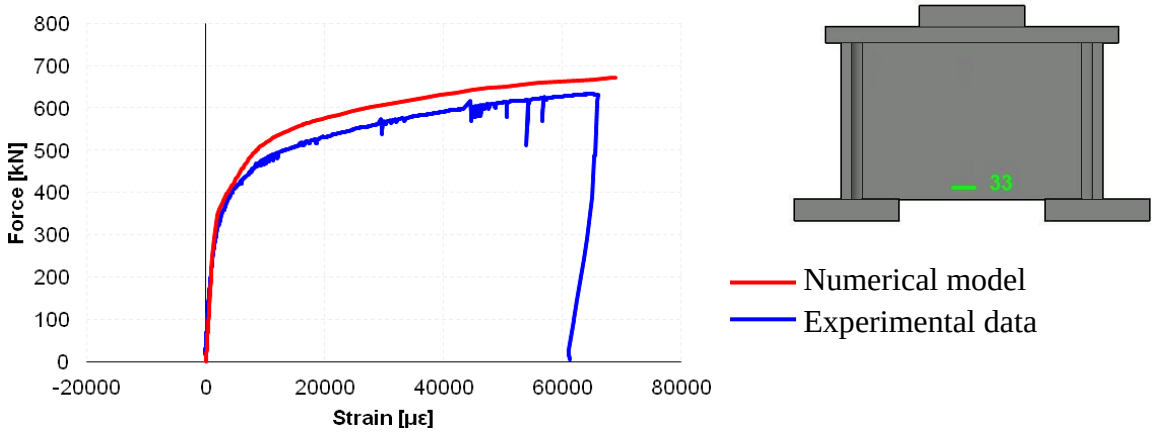

Figure 4.15 Force - strain response of Model 02 and Test02_2U_h100b80t8L210 obtained in the point 33.

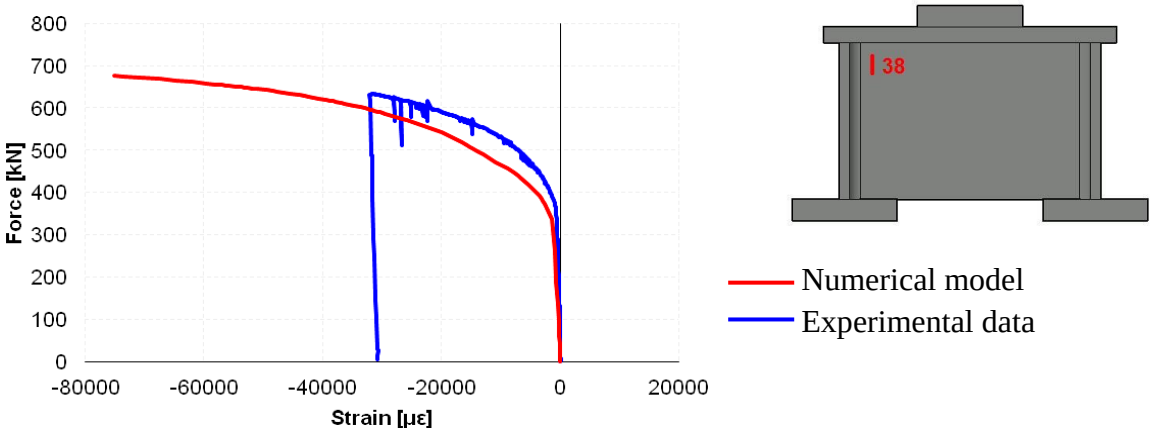

Figure 4.16 Force - strain response of Model 02 and Test02_2U_h100b80t8L210 obtained in the point 38.

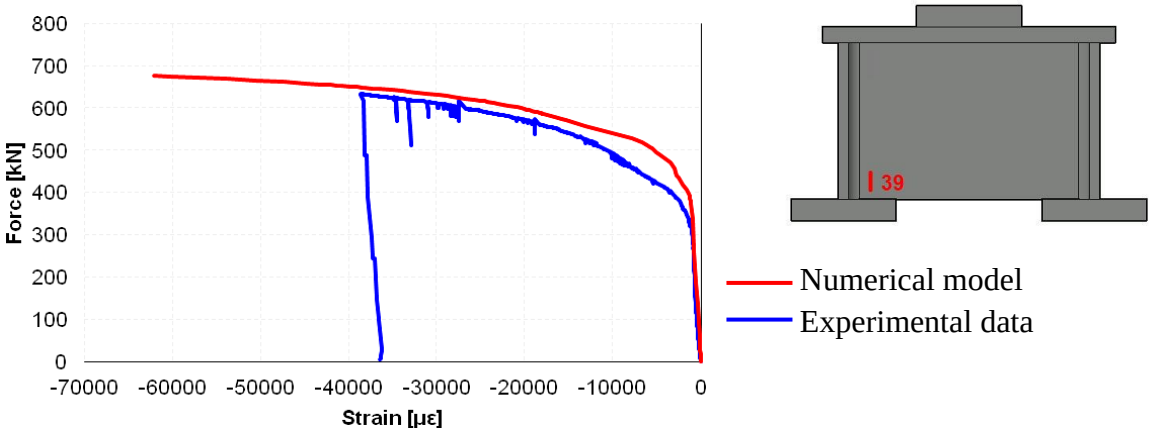

Figure 4.17 Force - strain response of Model 02 and Test02_2U_h100b80t8L210 obtained in the point 39.

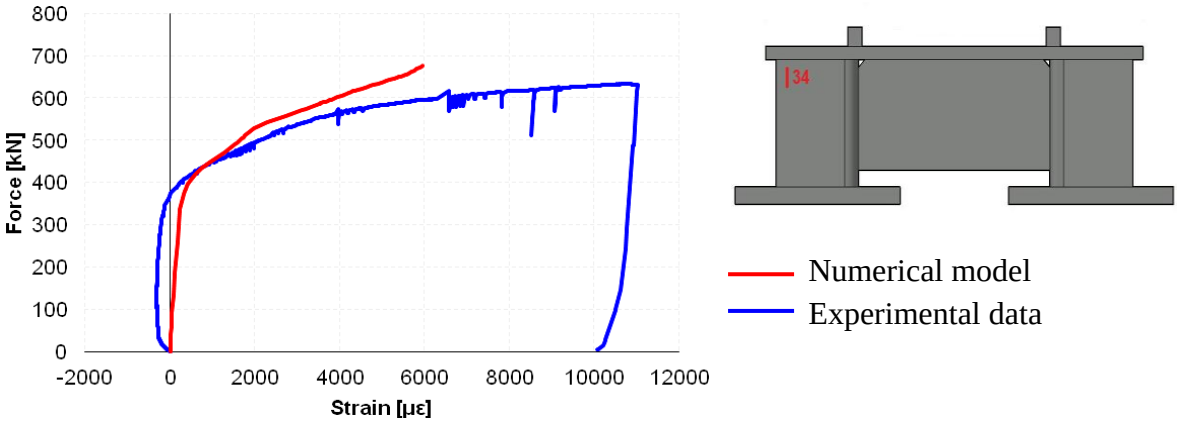

Figure 4.18 Force - strain response of Model 02 and Test02_2U_h100b80t8L210 obtained in the point 34.

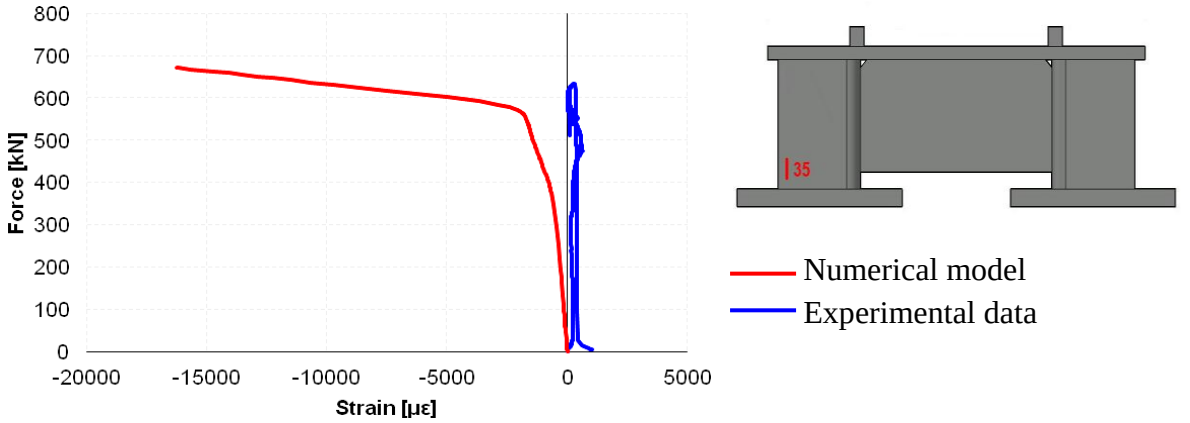

Figure 4.19 Force - strain response of Model 02 and Test02_2U_h100b80t8L210 obtained in the point 35.

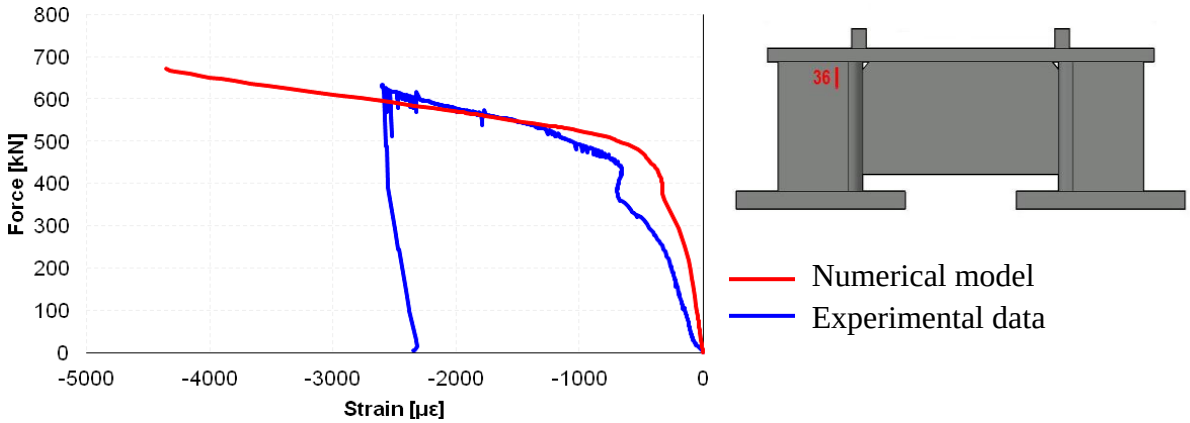

Figure 4.20 Force - strain response of Model 02 and Test02_2U_h100b80t8L210 obtained in the point 36.

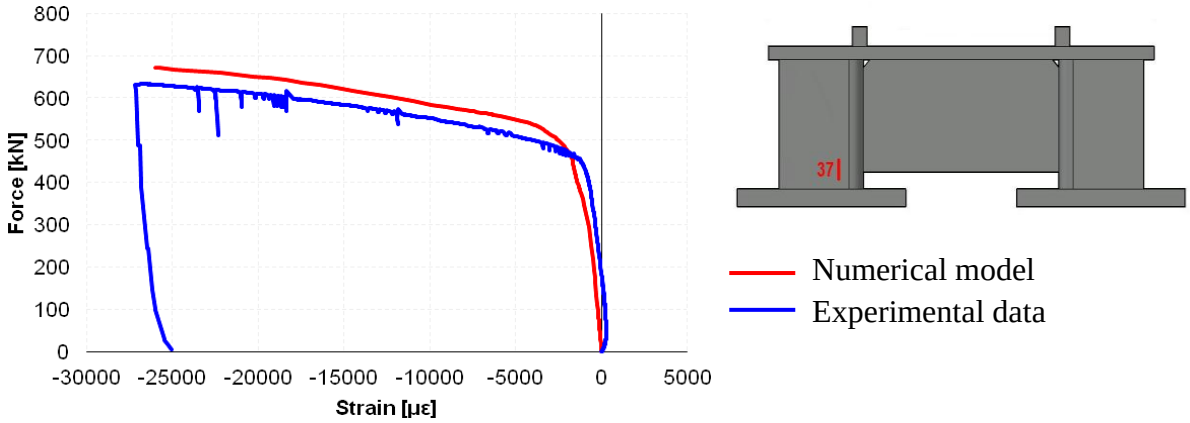

Figure 4.21 Force - strain response of Model 02 and Test02_2U_h100b80t8L210 obtained in the point 37.

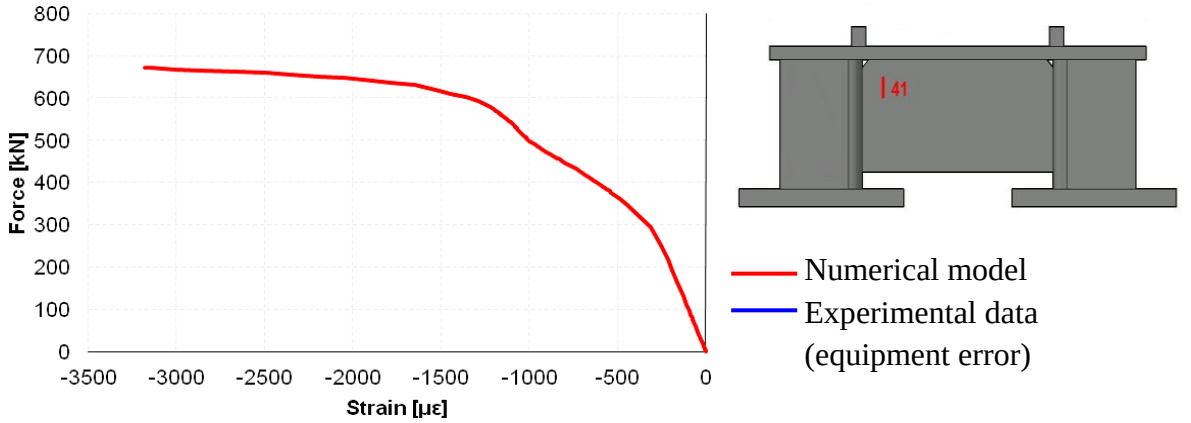

Figure 4.22 Force - strain response of Model 02 and Test02_2U_h100b80t8L210 obtained in the point 41.

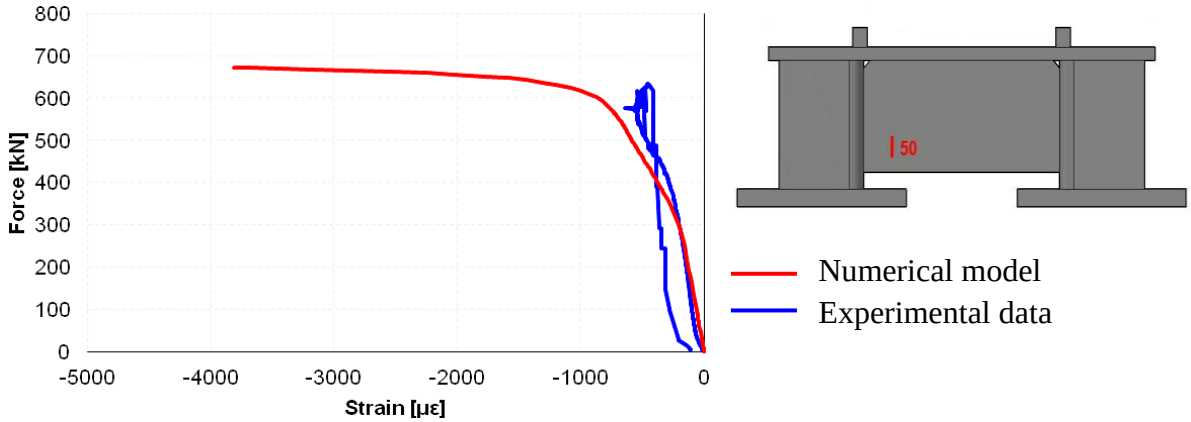

Figure 4.23 Force - strain response of Model 02 and Test02_2U_h100b80t8L210 obtained in the point 50.

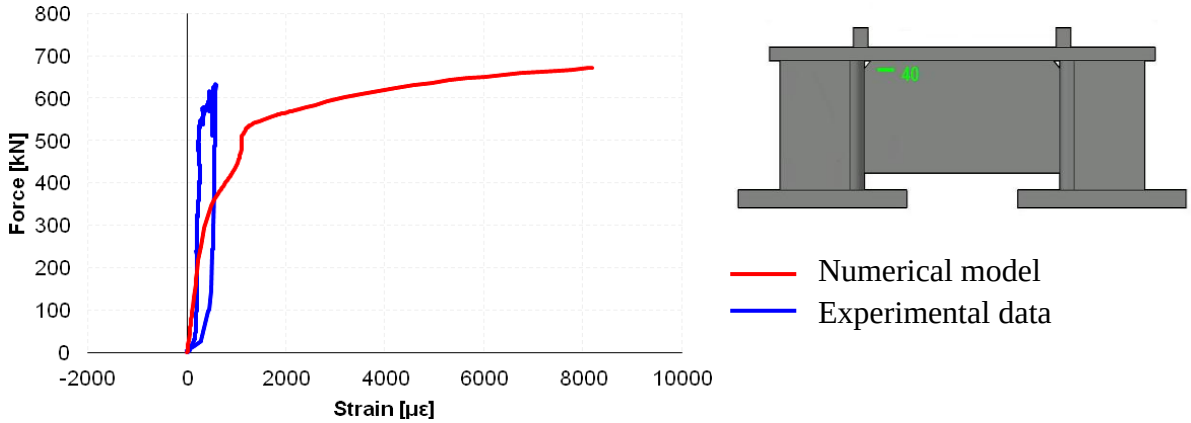

Figure 4.24 Force - strain response of Model 02 and Test02_2U_h100b80t8L210 obtained in the point 40.

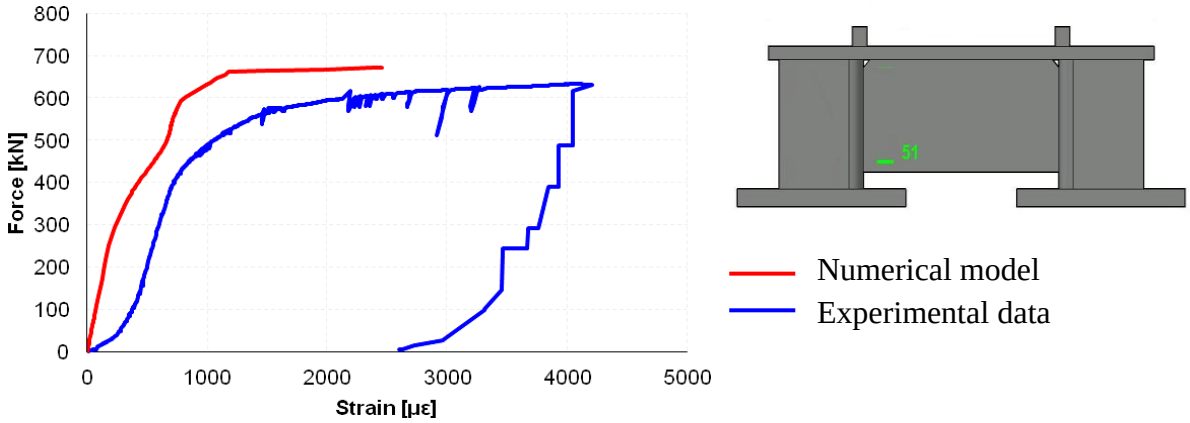

Figure 4.25 Force - strain response of Model 02 and Test02_2U_h100b80t8L210 obtained in the point 51.

In the Figure 4.12 to Figure 4.25 it is obvious that the force versus strain response of numerical model Model 01 shows a good agreement with the experimental specimen Test01_2U_h100b80t8L100.

The difference observed in numerical and experimental force - strain response in points 35, 40 and 50 could be explained by unstable experimental response. Considering the low level of strains in these points one may say that there is a difficulty in measuring low strains due to equipment sensibility and testing adjustment in the initial loading stage. By the same reason experimental force - strain curve in the point 41 was not evaluated.

Other three numerical models also perform the similar deformation response comparing to experimental force versus strain curves. Force versus strain diagrams for the Model 02 are provided for the most deformable points of the channel as they are the points of the highest interest. Diagrams are imaged in the Figure 4.26 to Figure 4.28.

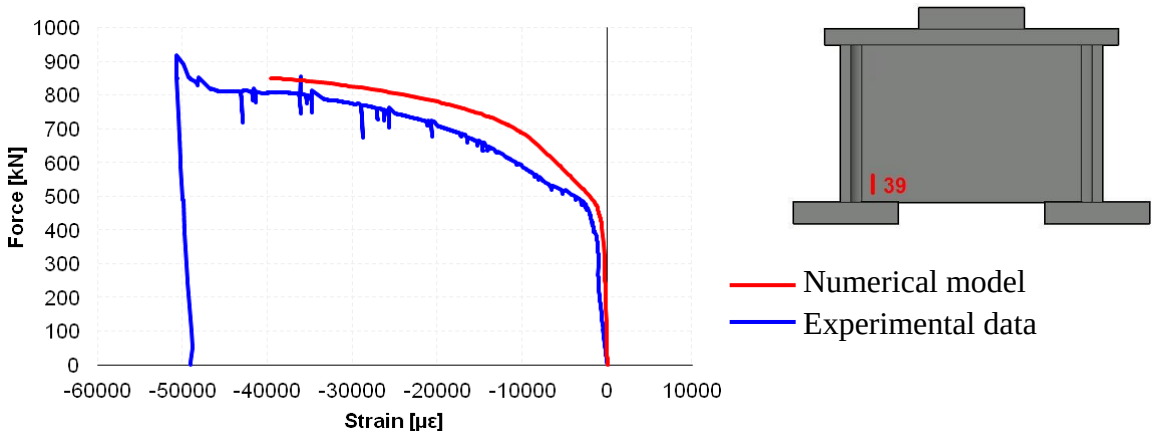

Figure 4.26 Force - strain response of Model 02 and Test02_2U_h100b80t8L210 obtained in the point 39.

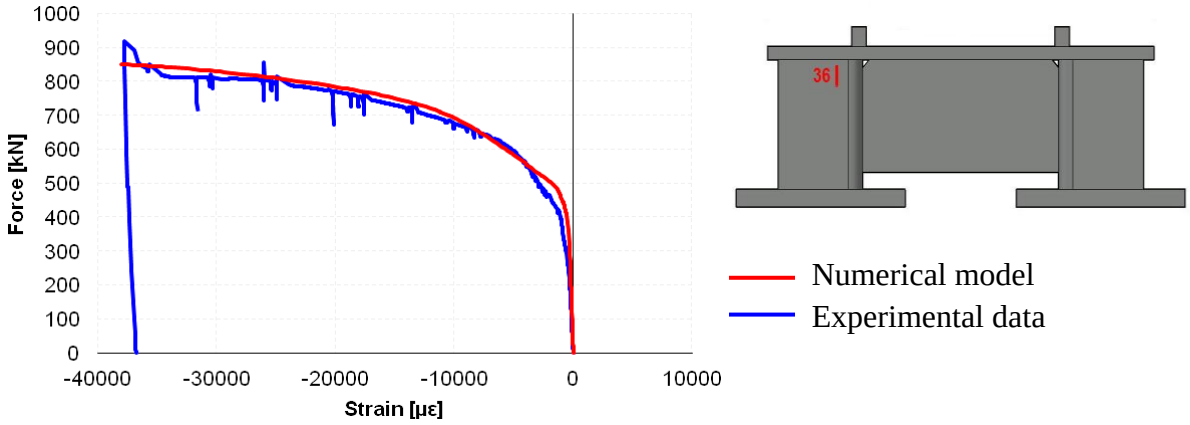

Figure 4.27 Force - strain response of Model 02 and Test02_2U_h100b80t8L210 obtained in the point 36.

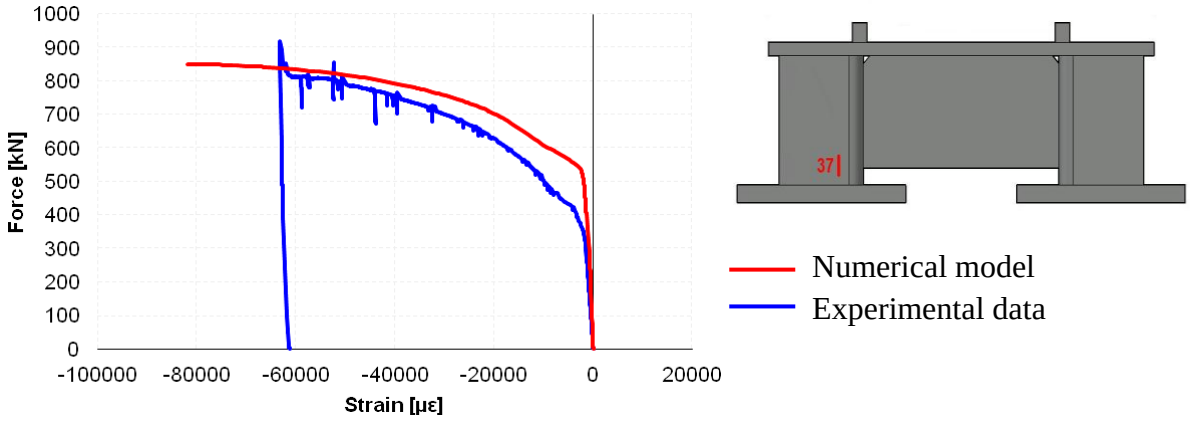

Figure 4.28 Force - strain response of Model 02 and Test02_2U_h100b80t8L210 obtained in the point 37.

Taking into consideration all mentioned above, results obtained numerically match with the experimental data what indicates that the accuracy of the finite element model needed for the calibration of the model is acceptable.

4.5. Parametric study. Results

In the frame of the present thesis the parametric study is evaluated for 104 model more based on those 4 numerical models which were previously calibrated by the comparison to experimental results. The overall number of numerical models of the parametric study is 108 models.

The variable parameters of the parametric study are as followed:

- U-section thickness (*t*),
- U-section height (*h*),
- U-section flange width (*B*),

- Loading plate length (L_{load}).

As the result of the parametric study resistance and stiffness coefficient are evaluated and listed in the Table 4.4 to Table 4.6 (U-section height is 100 mm) and the Table 4.7 to Table 4.9 (U-section height is 150 mm).

Table 4.4 Parametric study of numerical models 1 to 18.

Model name	U-section			Loading plate	Analysis output	
	Height	Width	Thickness	Length	Resistance	Stiffness coefficient
	h	B	t	L_{load}	F_{Rd}	k
	[mm]	[mm]	[mm]	[mm]	[kN]	[mm]
1	100	80	6	80	368.75	2.50
2				100	384.35	2.62
3				140	404.47	3.25
4				160	417.86	3.44
5				210	442.41	3.93
6				250	451.04	4.32
7			8	80	468.36	2.83
Model01				100	487.96	3.02
9				140	528.32	3.61
10				160	546.49	4.00
Model02				210	590.89	4.72
12				250	605.54	5.14
13			10	80	671.03	4.23
14				100	700.65	4.49
15				140	764.53	4.97
16				160	797.25	5.22
17				210	866.81	5.84
18				250	890.97	6.64

Table 4.5 Parametric study of numerical models 19 to 36.

Model name	U-section			Loading plate	Analysis output	
	Height	Width	Thickness	Length	Resistance	Stiffness coefficient
	h	B	t	L_{load}	F_{Rd}	k
	[mm]	[mm]	[mm]	[mm]	[kN]	[mm]
19	100	100	6	80	384.27	2.43
20				100	397.25	2.66
21				140	422.19	3.30
22				160	440.83	3.50
23				210	476.88	4.02
24				250	488.94	4.44
25			8	80	501.83	3.11
26				100	513.66	3.53
27				140	568.21	3.86
28				160	587.90	4.25
29				210	656.28	4.59
30				250	678.10	5.16
31			10	80	697.76	3.95
32				100	718.50	4.57
33				140	789.55	5.08
34				160	829.16	5.33
35				210	920.51	5.99
36				250	967.74	6.51

Table 4.6 Parametric study of numerical models 37 to 54.

Model name	U-section			Loading plate	Analysis output	
	Height	Width	Thickness	Length	Resistance	Stiffness coefficient
	h	B	t	L_{load}	F_{Rd}	k
	[mm]	[mm]	[mm]	[mm]	[kN]	[mm]
37	100	120	6	80	392.05	2.45
38				100	405.40	2.69
39				140	449.07	2.95
40				160	451.70	3.54
41				210	494.93	4.07
42				250	517.02	4.51
43			8	80	511.85	3.13
44				100	518.99	3.70
45				140	581.67	3.90
46				160	607.91	4.22
47				210	680.68	4.70
48				250	717.96	5.24
49			10	80	694.27	4.35
50				100	732.65	4.62
51				140	806.67	5.14
52				160	849.09	5.40
53				210	952.10	6.09
54				250	1005.77	6.99

Table 4.7 Parametric study of numerical models 55 to 72.

Model name	U-section			Loading plate	Analysis output	
	Height	Width	Thickness	Length	Resistance	Stiffness coefficient
	h	B	t	L_{load}	F_{Rd}	k
	[mm]	[mm]	[mm]	[mm]	[kN]	[mm]
55	150	120	6	80	523.94	2.93
56				100	533.27	3.30
57				140	565.00	3.69
58				160	581.97	3.85
59				210	611.02	4.23
60				250	614.58	4.71
61			8	80	672.68	3.84
62				100	700.17	4.16
63				140	753.96	4.52
64				160	769.04	4.97
65				210	825.12	5.25
66				250	823.76	6.14
67			10	80	902.49	4.67
Model03				100	973.40	4.93
69				140	1060.89	5.67
70				160	1090.55	6.15
Model04				210	1178.85	6.44
72				250	1188.08	7.49

Table 4.8 Parametric study of numerical models 73 to 90.

Model name	U-section			Loading plate	Analysis output	
	Height	Width	Thickness	Length	Resistance	Stiffness coefficient
	h	B	t	L_{load}	F_{Rd}	k
	[mm]	[mm]	[mm]	[mm]	[kN]	[mm]
73	150	150	6	80	520.80	3.27
74				100	539.54	3.45
75				140	580.29	3.77
76				160	602.28	3.92
77				210	639.36	4.51
78				250	656.33	4.85
79			8	80	670.19	4.24
80				100	701.56	4.48
81				140	757.57	4.92
82				160	790.22	5.08
83				210	857.51	5.61
84				250	889.62	5.99
85			10	80	899.51	4.99
86				100	983.25	5.07
87				140	1082.17	5.80
88				160	1108.71	6.50
89				210	1210.75	7.22
90				250	1263.39	7.75

Table 4.9 Parametric study of numerical models 91 to 108.

Model name	U-section			Loading plate	Analysis output	
	Height	Width	Thickness	Length	Resistance	Stiffness coefficient
	h	B	t	L_{load}	F_{Rd}	k
	[mm]	[mm]	[mm]	[mm]	[kN]	[mm]
91	150	180	6	80	525.41	3.30
92				100	544.24	3.48
93				140	586.50	3.80
94				160	608.55	3.97
95				210	654.47	4.40
96				250	665.99	4.93
97			8	80	674.55	4.28
98				100	706.71	4.53
99				140	763.81	4.98
100				160	796.74	5.14
101				210	866.14	5.69
102				250	886.64	6.45
103			10	80	914.56	4.77
104				100	988.50	5.13
105				140	1090.41	5.89
106				160	1139.61	6.08
107				210	1220.59	7.36
108				250	1275.84	7.92

For getting the better image of the obtained results the data is presented graphically in the Figure 4.29 to Figure 4.31 which follow below.

In the diagrams presented in the Figure 4.29 to Figure 4.31, each line consists of 6 points which correspond to the resistance and the stiffness coefficient obtained for different length of the loading plates (L_{load}) 80 mm, 100 mm, 140 mm, 160 mm, 210 mm and 250 mm. In each diagram U-section thickness is invariable.

From resistance versus stiffness coefficient graphs it can be concluded that for the invariable channel geometry the increasing of the loading plate length leads to increase of resistance and stiffness of the component. Herein, the loading plate represents the zone loaded in compression such as the flange of a I-beam.

Furthermore, one may notice that increase of the channel flange width does not improve the component mechanical response. Opposite to the flange width, increase of the channel height enhances resistance and stiffness of the component. This fact can be proved by comparing graphs of U-sections of the same flange width namely B = 120 mm and of the different height (Figure 4.29 to Figure 4.31).

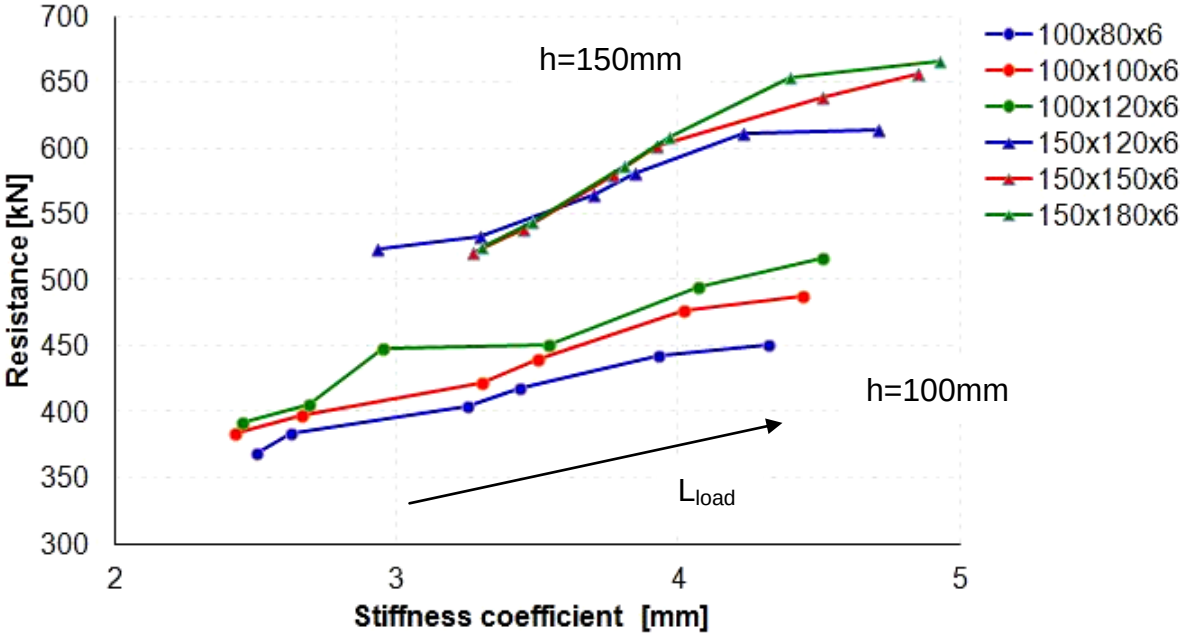

Figure 4.29 Resistance - stiffness coefficient relation for compression components (channel thickness equals to 6 mm).

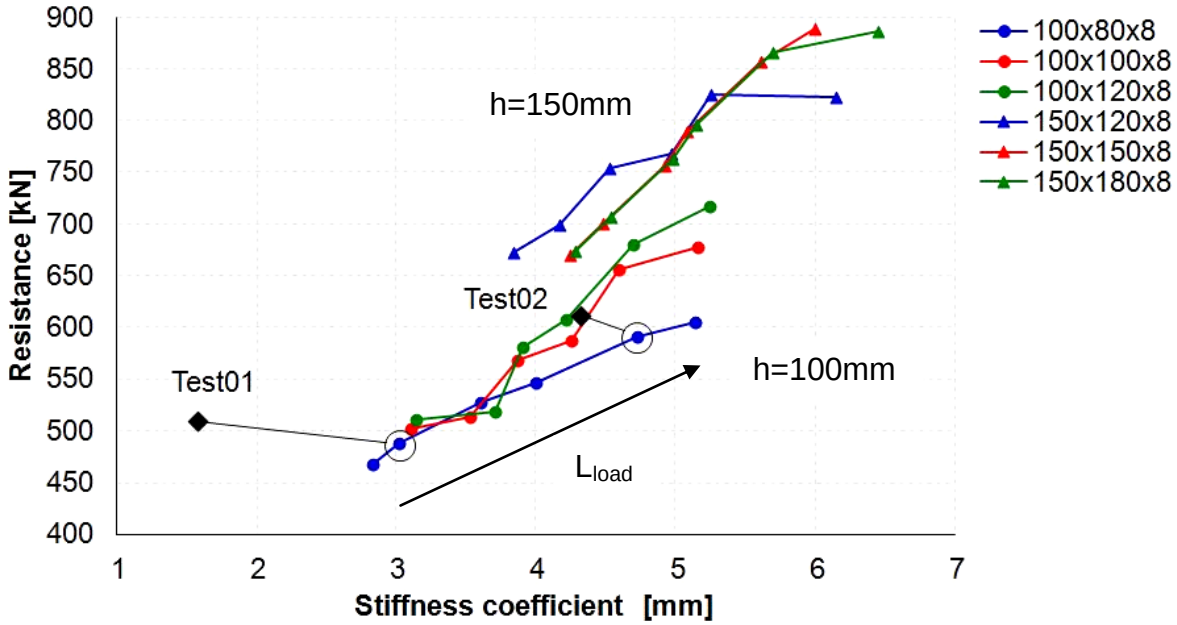

Figure 4.30 Resistance - stiffness coefficient relation for compression components (channel thickness equals to 8 mm).

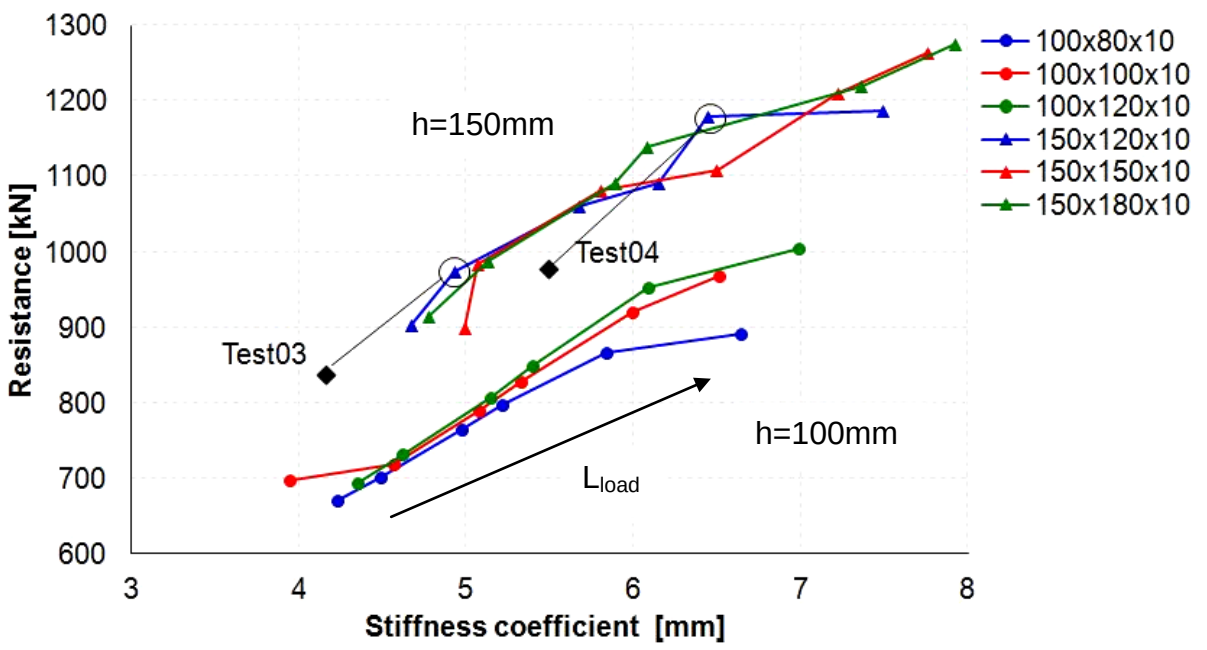

Figure 4.31 Resistance - stiffness coefficient relation for compression components (channel thickness equals to 10 mm).

One more parameter strongly affecting both resistance and stiffness is the U-section thickness. Increase of the thickness leads to the better mechanical performance of the component. This dependence can be observed in the Figure 4.32 to Figure 4.33.

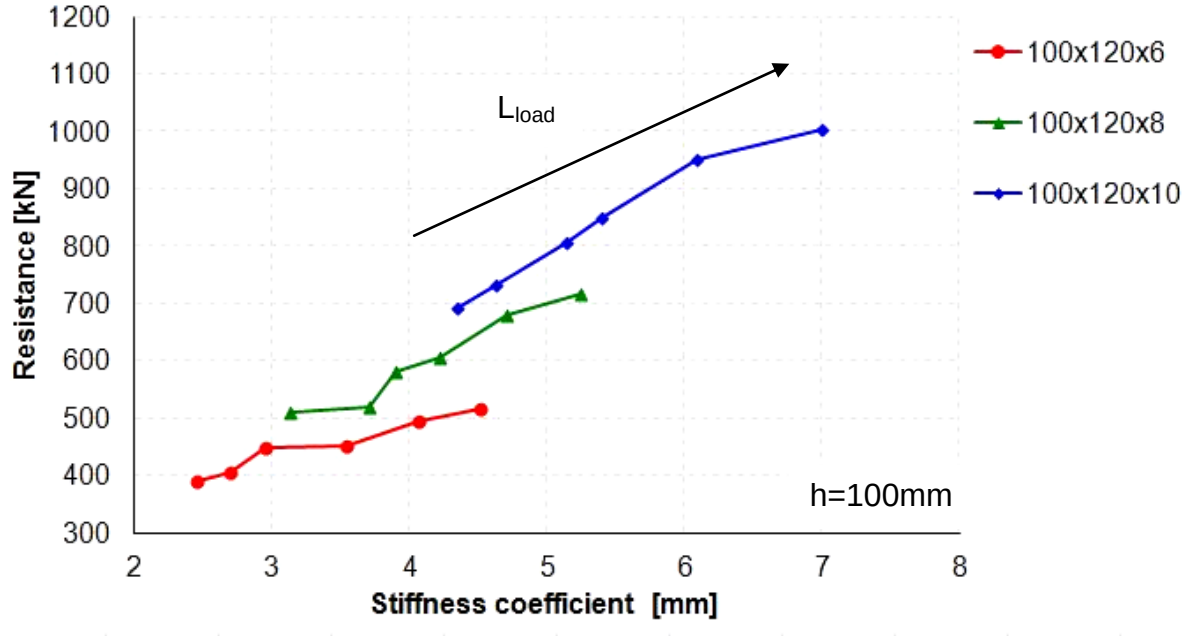

Figure 4.32 Resistance - stiffness coefficient relation for compression components (channel height and flange width are fixed, *h*=100 mm, *B*=120 mm, thickness is variable).

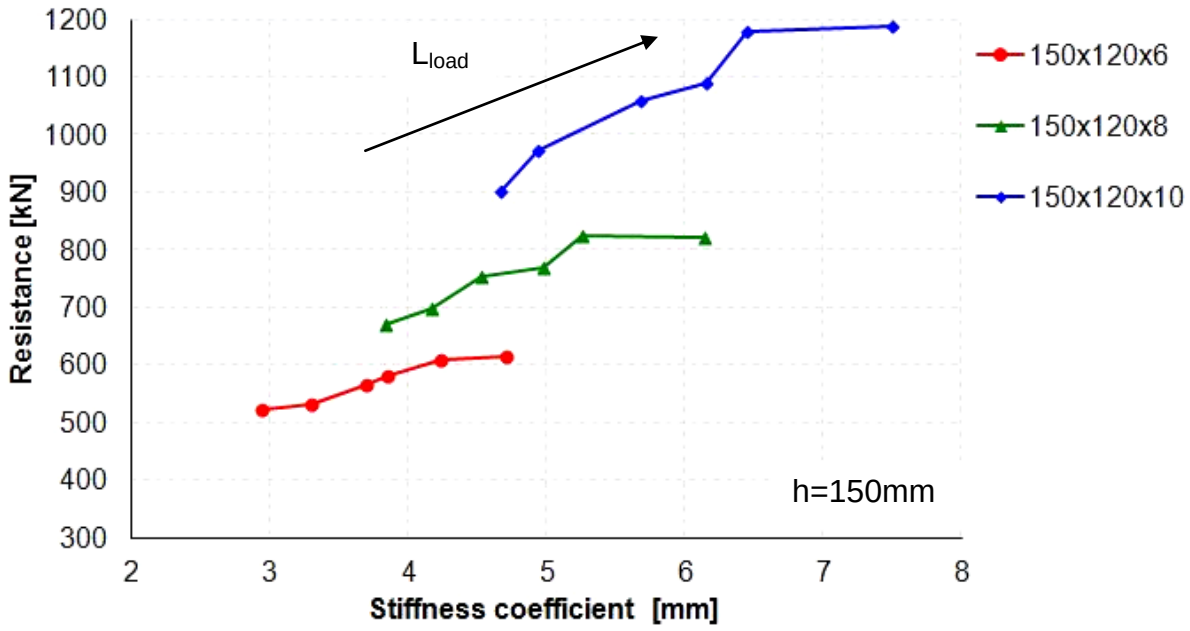

Figure 4.33 Resistance - stiffness coefficient relation for compression components (channel height and flange width are fixed, *h*=150 mm, *B*=120 mm, thickness is variable).

4.6. Parametric study. Mechanical behaviour

Implementation of the parametric study has detected several sequences of the mechanical behaviour of the component. These sequences are highlighted in the present chapter.

Analysing numerical models 1 to 6 (*h*=100 mm, *B*=80 mm, *t*=6 mm) (Figure 4.34 to Figure 4.39) which are loaded through loading plates of variable length (80 mm to 250 mm) one may conclude that increase of the loading plate length leads to redistribution of stresses from the U-section web to the U-section flanges. It happens due to different response of the end-plate (top horizontal plate in the pictures).

Shorter loading plate length causes significant transversal bending of the end-plate. Thus, it's edges lift up and partially unload U-section flanges from compression while the U-section web is in bending. The stresses distribution for the shortest loading plate length is depicted in the Figure 4.34.

Provided increase of the loading plate length, the end-plate is loaded in compression through the larger area what leads to more uniform distribution of compressive stresses throughout the end-plate in the transversal direction. Therefore, the U-section flanges are a subject of higher stresses and deformations. In the Figure 4.39 the stresses distribution for the longest loading plate length is imaged. From the deformed shape of the channel it can be observed that flanges lose local stability near the free edges.

In all the cases the effect of the vertical stiffener is observed. It provides additional stiffness to the U-section web.

However, components loaded through the longer loading plate demonstrate higher resistance and stiffness. This type of behaviour is valid for the whole range of the studied numerical models.

Stiffness of the component increases by 5% increasing the loading plate length from 80 mm to 100 mm and by 73% from 80 mm to 250 mm.

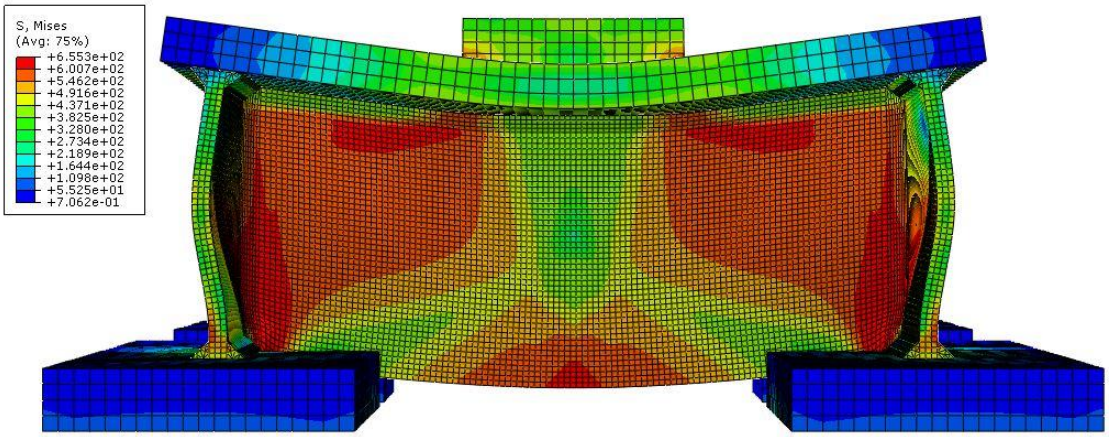

Figure 4.34 Stress distribution in the Model 1 (L_{load} = 80 mm).

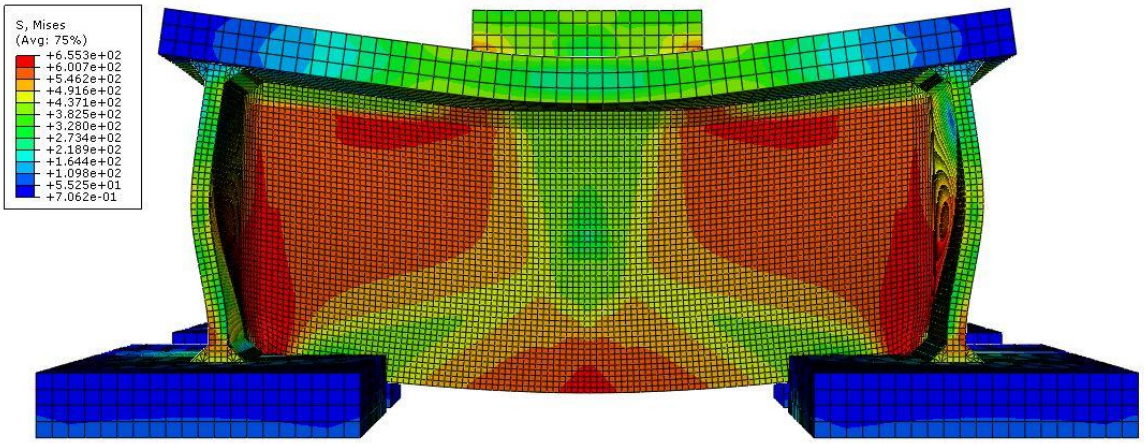

Figure 4.35 Stress distribution in the Model 2 (L_{load} = 100 mm).

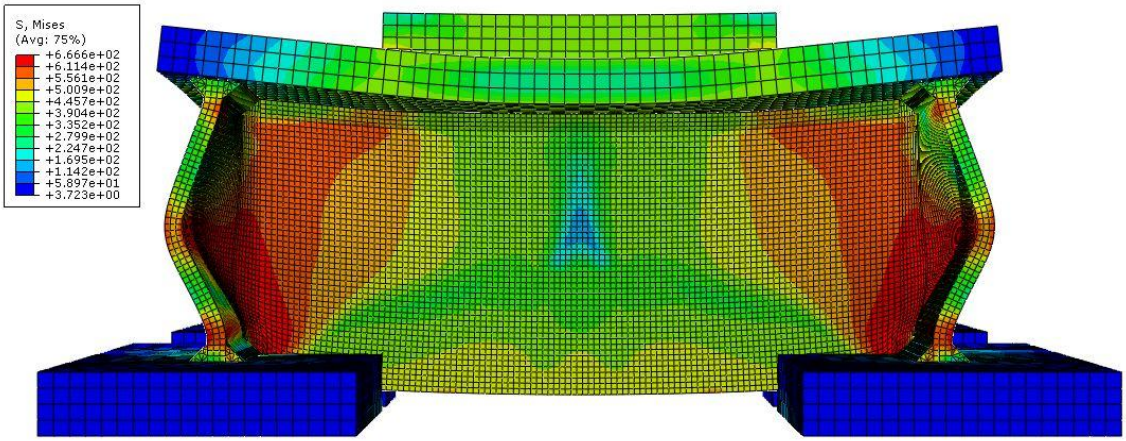

Figure 4.36 Stress distribution in the Model 3 (L_{load} = 140 mm).

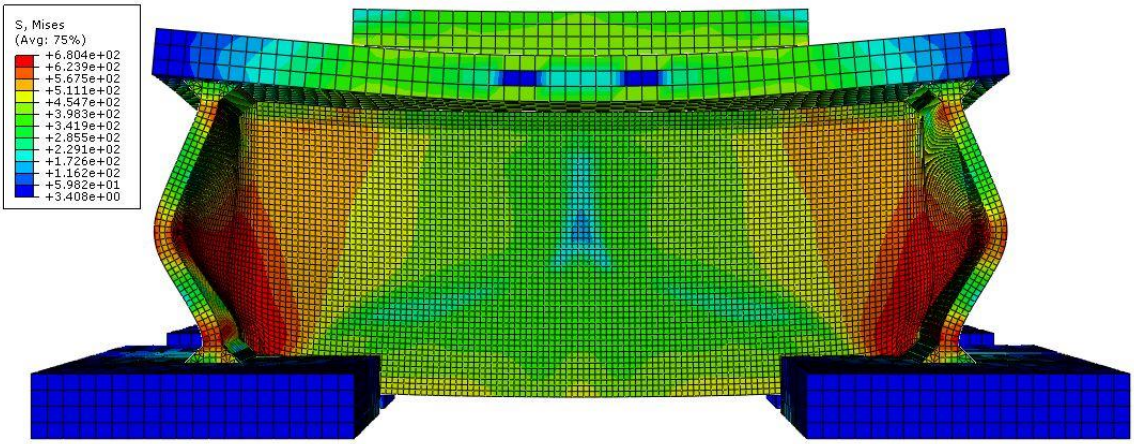

Figure 4.37 Stress distribution in the Model 4 (L_{load} = 160 mm).

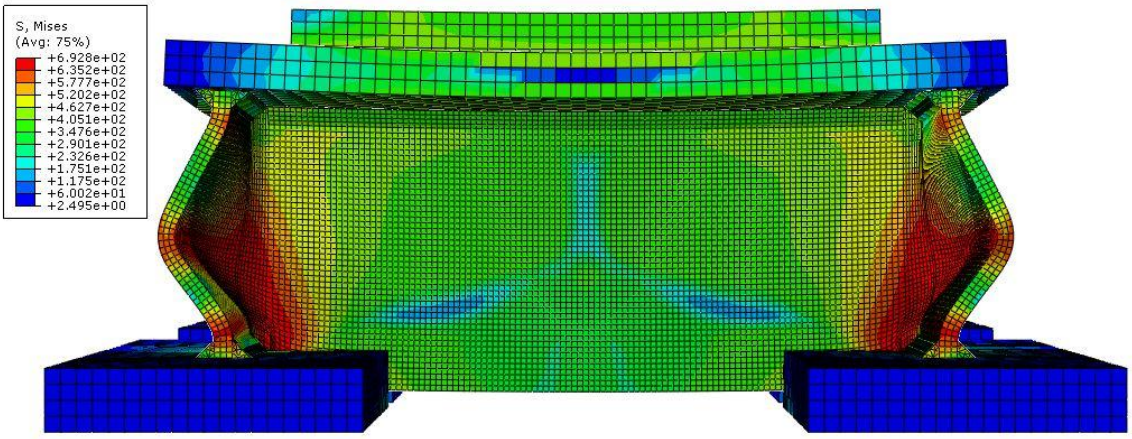

Figure 4.38 Stress distribution in the Model 5 (L_{load} = 210 mm).

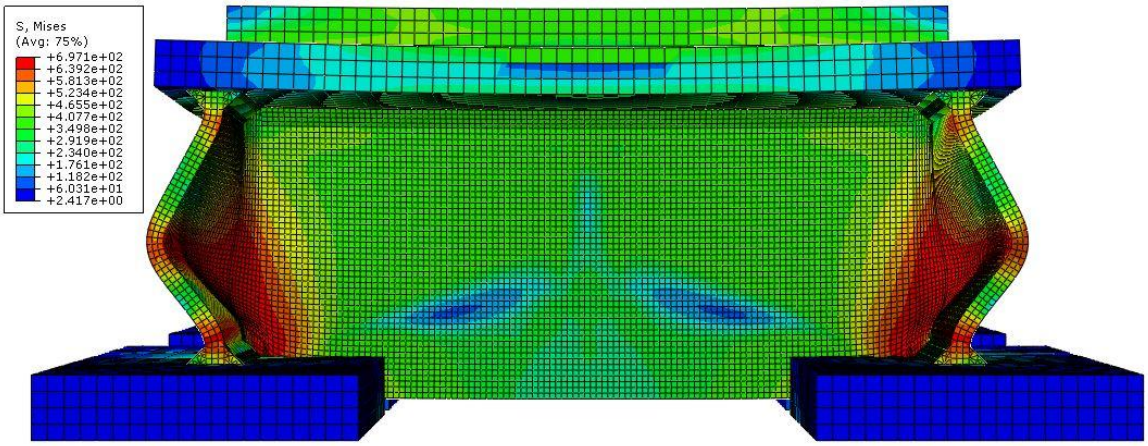

Figure 4.39 Stress distribution in the Model 6 (L_{load} = 250 mm).

Varying the channel thickness and keeping other geometrical parameters constant one may conclude that increase of the thickness increases stresses concentrated in the channel web and decreases stresses in the channel flanges. This effect is depicted in the Figure 4.40 to Figure 4.42 on the example of three numerical models (h=100 mm, B=80 mm, L_{load} = 80 mm) with variable thickness. Deformation of the U-section decreases with increasing thickness. Resistance and stiffness tend to increase provided increase of the U-section thickness.

Stiffness of the component increases by 13% increasing the channel thickness from 6 mm to 8 mm and by 69% from 6 mm to 10 mm.

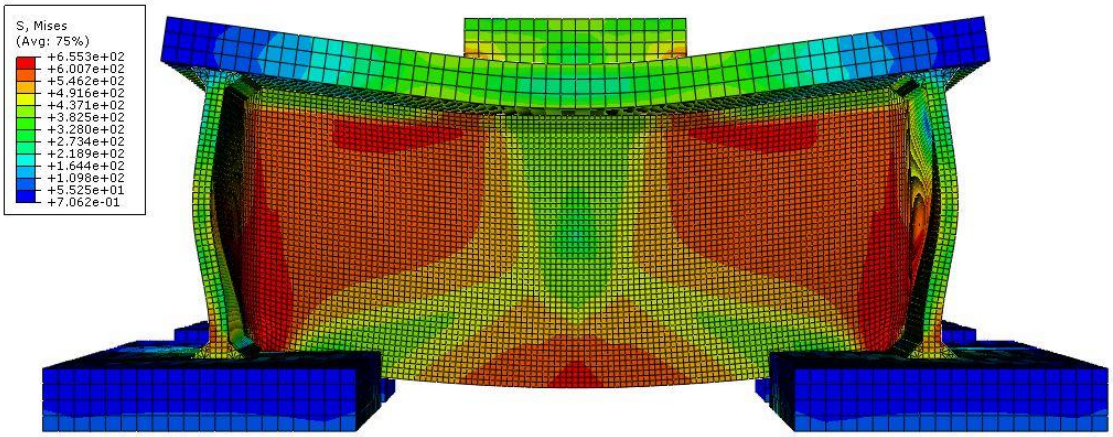

Figure 4.40 Stress distribution in the Model 1 (t = 6 mm).

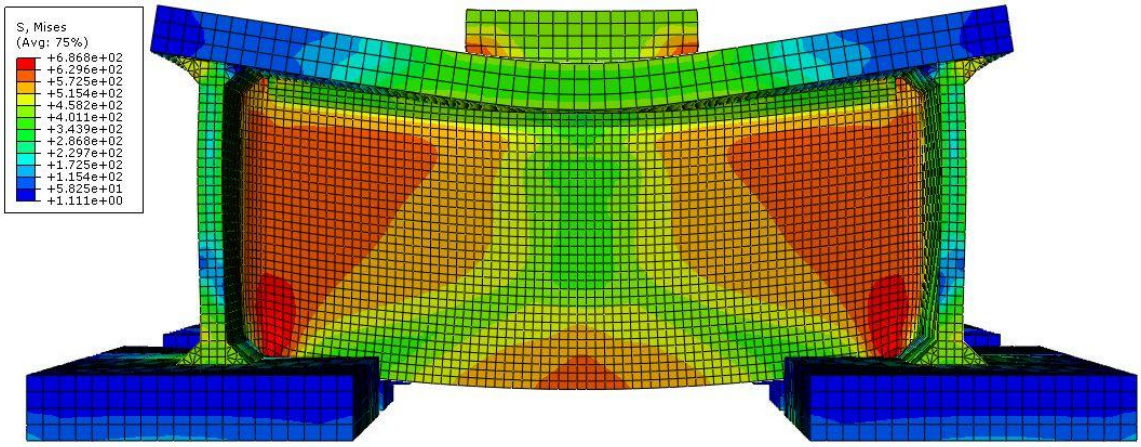

Figure 4.41 Stress distribution in the Model 7 (t = 8 mm).

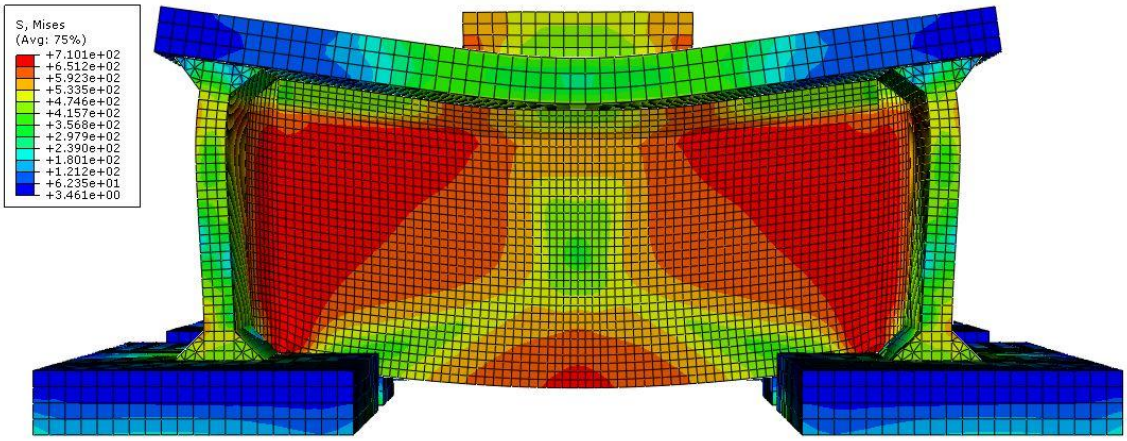

Figure 4.42 Stress distribution in the Model 13 (t = 10 mm).

5.CONCLUSION

5.1. Conclusion

The main goal of present thesis is development of an appropriate numerical model which could describe the behaviour of the compressed component of the beam-to-rectangular hollow section column moment resistant steel joint.

Such a numerical model is designed using *DS Simulia Abaqus* software and validated by comparison to experimental results previously obtained by laboratory tests. The tests were carried out for four specimens under the monotonic compressive load.

After the calibration of obtained results, the parametric study of 104 numerical models more is implemented in order to investigate the behaviour for the extended range of geometrical variety of the beam-to-RHS column joint.

The parametric study presents values of the resistance and stiffness coefficient of the compressed component depending on the channel thickness, height, flange width and length of the loaded area. These results will be useful for the calibration of the analytical model that can come to be developed in the scope of the previously referred research project.

Obtained results are consistent and show strength and stiffness growth consequent from the increase of any of listed parameters. Although, the most significant strength and stiffness enhance is caused by increase of the channel thickness and the loading plate length.

Taking into consideration the set of obtained results, the compressed component performs high strength and high stiffness.

5.2. Future work

Considering the present thesis as a part of the wider research project, namely numerical analysis of the compressed component of the moment resistant joint, the future work includes numerical analysis of the tensile component and then the beam-to-RHS column joint.

Obtained results are supposed to serve for analysing the joint behaviour and developing an analytical solution. It will describe the behaviour of basic joint components based on the concept of the component method which is widely applied in existing codes.

Implementation of design guidelines aims to be included into codes through particular recommendations. Consequently, the design procedure is going to be much facilitated what will allow to apply hollow sections throughout.

6.REFERENCES

Barros dos Santos, G., Miranda Batista, E. de, Mascarenhas de Araujo, A.H., 2016: Behaviour of RHS beam-to-column bolted steel connections. Steel Construction 9 (2016), No.4. Berlin, Germany, pp. 296-304.

Dassault Systemes Simulia Corp., 2007: Abaqus analysis. User's manual. Version 6.7, USA.

EN 1090-2, 2008: execution of steel structures and aluminium structures - Part 2: Technical requirements for steel structures. European Committee for Standardization, CEN, Brussels.

EN 1993-1-8, 2005: Eurocode 3: Design of steel structures - Part 1-8: Design of joints. European Committee for Standardization, CEN, Brussels.

EN 10025-2, 2004: Hot rolled products of structural steels - Part 2: Technical delivery conditions for non-alloy structural steels. European Committee for Standardization, CEN, Brussels.

EN 10210-1, 2006: Hot finished structural hollow sections of non-alloy and fine grain steels - Part 1: technical delivery conditions. European Committee for Standardization, CEN, Brussels.

Faella, C., Piluso, V., Rizzano, G., 1999: Structural steel semirigid connections: theory, design and software. Boca Raton, Florida, CRC Press.

Hoang, V.L., Jaspart, J.-P., Demonceau, J.-F., 2016: Use of long bolts for beam-to-concrete-filled rectangular hollow section column joints in seismic-resistant frames. Steel Construction 9 (2016), No.4. Berlin, Germany, pp. 305-314.

Jaspart, J.P., Pietrapertosa, C., Weynand, K., Busse, E., Klinkhammer, R., 2005: Development of a full consistent design approach for bolted and welded joints in building frames and trusses between steel members made of hollow and/or open sections. Application of the component method. Draft final report - Volume 1. Practical design guide, Research Project 5BP, CIDECT.

Khador, M., Chan, T.-M., 2016: Cyclic behaviour of external diaphragm joint to CHS column with built-in replaceable links. Steel Construction 9 (2016), No.4. Berlin, Germany, pp. 331-338.

Kurobane, Y., Packer, J.A., Wardenier, J., Yeomans, N., 2004: Design guide for structural hollow section column connections. CIDECT, Koln, Germany.

Lopes, F., Santiago, A., Simoes da Silva, L., Heistermann, T., Veljkovic, M., Silva, J.G. da, 2013: Experimental behaviour of the reverse channel joint component at elevated and ambient temperatures. International Journal of Steel Structures, September 2013, Vol 13, No 3, pp. 459-472.

Packer, J.A., Wardenier, J., Zhao, X.-L., Vegte, G.J. van der, Kurobane, Y., 2009: Design guide for rectangular hollow section (RHS) joints under predominantly static loading. 2nd edition. CIDECT, Geneva, Switzerland.

Puthli, R., Herion, S., 3-5 April 2001: Tubular structures IX: Proceedings of the Ninth International Symposium and Euroconference on tubular structures. Dusseldorf, Germany.

Sabbagh, A.B., Chan, T.M., Mottram, J.T.: Detailing of I-beam-to-CHS column joints with external diaphragm plates for seismic actions. Journal of Constructional Steel Research, Elsevier Science Ltd. 88 (2013), pp. 21-33.

Silva, L.S. da, L., Santiago, A., Lopes, F., Heistermann, T., Veljkovic, M., Igbal, N., Wald, F., Jana, T., Davison, B., Burgess, I., Huang, S.-S., Dong, G., Wang, Y., Mandal, P., Hu, Y., Jafarian, M., Koutlas, G., 2011: COMPFIRE: Design of composite joints for improved fire robustness. Mid-term Technical Implementation report No. 2, Research Fund for Coal and Steel, European Commission, Brussels.

Vicente, G.S.F., Simoes, R.A.D., Rebelo, C.A.S., Silva, L.S. da, Veljkovic, M., 2014: Moment resisting bolted joints connecting steel tubular sections. EUROSTEEL 2014, September 10-12, 2014, Naples, Italy.

Wardenier, J., Packer, J.A., Zhao, X.-L., Vegte, G.J. van, 2010: Hollow sections in structural applications. 2nd edition, CIDECT, Geneva, Switzerland.